Inorg. Chem. **2008**, *47*, 413–428

Self-assembly of Ligands Designed for the Building of a New Type of [2 × 2] Metallic Grid. Anion Encapsulation and Diffusion NMR Spectroscopy

Blanca R. Manzano,*,† Félix A. Jalón,† Isabel M. Ortiz,† M. Laura Soriano,† Felipe Gómez de la Torre,† José Elguero,‡ Miguel A. Maestro,§ Kurt Mereiter,|| and Tim D. W. Claridge⊥

Departamento de Química Inorgánica, Orgánica y Bioquímica, Facultad de Químicas, IRICA, Universidad de Castilla-La Mancha, Avda Camilo José Cela, 10, E-13071 Ciudad Real, Spain, Instituto de Química Médica, Centro de Química Orgánica 'Manuel Lora-Tamayo', CSIC, Juan de la Cierva 3, E-28006 Madrid, Spain, Servicios Xerais de Apoio á Investigación, Universidad de A Coruña, Campus de A. Zapateira, E-15071 A Coruña, Spain, Faculty of Chemistry, Vienna University of Technology, Getreidemarkt 9/164 SC, A-1060 Vienna, Austria, Chemistry Research Laboratory, Department of Chemistry, University of Oxford, Mansfield Road, Oxford, OX1 3TA, UK

Received June 7, 2007

The ligands 4,6-bis(pyrazol-1-yl)pyrimidine (bpzpm), 4,6-bis(3,5-dimethylpyrazol-1-yl)pyrimidine (bpz*pm), 4,6-bis-(4-methylpyrazol-1-yl)pyrimidine (Mebpzpm), and 3,6-bis(3,5-dimethylpyrazol-1-yl)pyridazine (ppdMe) were synthesized and were made to react with Cu(I) centers in the presence of different counteranions. Different [2 × 2] metallic grids were obtained. With ligands bpzpm, bpz*pm, and Mebpzpm, a new type of grid was obtained where the facing ligands were divergent and two counteranions (BF_4^- or PF_6^-) were hosted in the resulting cavities and exhibit C–H···F and anion···π interactions in the solid state. The presence of methyl groups on the pyrazolyl rings induced several distortions in the structure. In complexes with the ligand ppdMe, there were found two groups of parallel ligands in the grid, and the cavities generated were smaller. The counteranions were situated outside the grid, and the facing ligands exhibited aromatic π–π stacking interactions. Anion–π interactions involving the pyridazine ring were found. The behavior in solution of the new derivatives with a special emphasis on the cation–anion interactions was studied by UV–vis and NMR spectroscopy. Diffusion NMR experiments performed for some complexes allowed us to conclude that weak cation–anion interactions exist in solution, with the counteranions undergoing fast exchange on the diffusion time scale between the free and ion-paired states.

Introduction

There is a great interest in developing strategies for the synthesis of complex molecular architectures that could exhibit new properties and potential applications in nanotechnology. During the past few years, supramolecular chemistry, with the development of self-assembly processes, has provided important achievements in this direction.[1] Whereas the self-assembly of organic components has been a traditional area, the synthesis of inorganic architectures from organic ligands and metal ions is nowadays a very active area. The spontaneous generation of supramolecular entities is based on metal-ion-directed self-assembly, with the organic ligands having encoded information that is mainly related to the arrangement of the binding sites.[2,3] Different authors have recently presented[4] overviews in supramolecular inorganic building on the basis of the idea that different coordination geometries enable the controlled design of

* To whom correspondence should be addressed. E-mail: Blanca.Manzano@uclm.es. Fax: (internat.) + 34-926/295318.
† Universidad de Castilla-La Mancha.
‡ Centro de Química Orgánica 'Manuel Lora-Tamayo'.
§ Universidad de A Coruña, Campus de A. Zapateira.
|| Vienna University of Technology.
⊥ University of Oxford.

(1) Lehn, J.-M. *Supramolecular Chemistry - Concepts and Perspectives*; VCH, Weinheim: Weinheim, Germany, 1995.
(2) Baxter, P. N. M. In *Comprehensive Supramolecular Chemistry*; Atwood, J. L., Davies, J. E. D., MacNicol, D. D., Vögtle, F., Lehn, J.-M., Eds.; Pergamon Press: Oxford, U.K.; Vol. 9, pp 165−211.; Constable, E. C. in the same reference, pp 213−252; Fujita, M. in the same reference, pp 253−282.
(3) Ward, M. D. *Annu. Rep. Prog. Chem. Sect. A* **2001**, *97*, 293.

10.1021/ic701117a CCC: $40.75
Published on Web 10/02/2007

macrostructures. The functions and potential applications of such supramolecular entities for example as sensors in different electronic devices, in catalysis, etc. are also receiving increasing attention.[5] The encapsulation of molecules, cations, or anions has also been considered an important topic in this area.[6−8]

There is a general interest in grid-type metal-ion architectures[9] mainly because the topologies of the metal arrays can generate interesting optical, redox, magnetic, or catalytic properties[9,10] and might even serve as the basis for the building of information storage devices. There has been described the deposition on substrates of grids that have been imaged by scanning tunneling microscopy[11] and even the generation of molecular motion by interconversion between a helical free ligand and rack or grid-type of complexes has been reported.[12] The grids can also accommodate species such as anions or molecules in their cavities.[9,13−15] Tetrahedral metallic centers were first used,[14−18] and copper (I)[14−16] or silver (I)[17] centers coordinated, for example, to multidentate polypyridine or pyridine-polypyridazine ligands are illustrative examples. However, other geometries such as octahedral[9,10,19,20] or square pyramidal[21] have also been shown to be useful for the self-assembly of a variety of building blocks. In all of the described examples of grid structures, the facing ligands are parallel.

In this work, we aimed to synthesize [2 × 2] grid-shaped structures on the basis of the self-assembly of Cu(I) centers and ditopic organic fragments. One of our goals was to obtain a new type of grid architecture with the facing ligands not being parallel but having open interplanar angles. This would create intramolecular cavities of different shapes than that encountered in other grid structures and could host other types of molecules, thereby offering the potential of broadening the scope of further work in this area. This supramolecule would be similar to a highly preorganized organic cavitand described by Cram et al.[22] comprising four dibenzofuran units (Chart 1) that contains two cleft- and collar-shaped cavities. Each half of the molecule can accommodate aromatic rings

(4) (a) Olenyuk, B.; Fechtenkötter, A.; Stang, P. J. *J. Chem. Soc., Dalton Trans*. **1998**, 1707. (b) Stang, P. J. *Chem.—Eur. J*. **1998**, *4*, 19. (c) Holliday, B. J.; Mirkin, C. A. *Angew. Chem., Int. Ed*. **2001**, *40*, 2022. (d) Fujita, M.; Umemoto, K.; Yoshizawa, M.; Fujita, N.; Kusukawa, T.; Biradha, K. *Chem. Commun*. **2001**, 509. (e) Papaefstathiou, G. S.; MacGillivray, L. R. *Coord. Chem. Rev*. **2003**, *246*, 169.

(5) (a) *Encyclopedia of Supramolecular Chemistry*; Atwood, J. L., Steed, J. W., Eds.; Marcel Dekker, Inc.: New York, 2004. (b) Würthner, F.; You, C.-C.; Saha-Möller, C. R. *Chem. Soc. Rev*. **2004**, *33*, 133. (c) Janiak, C. *Dalton Trans*. **2003**, 2781. (d) Pri-Bar, I.; Koresh, J. E. *J. Mol. Catal. A.: Chem*. **2000**, *156*, 173. (e) Hofmeier, H.; Schubert, U. S. *Chem. Soc. Rev*. **2004**, *33*, 373. (f) Rudkevich, D. M. *Angew. Chem., Int. Ed*. **2004**, *43*, 558. (g) Fabrizzi, L.; Poggi, A. *Chem. Soc. Rev*. **1995**, 197. (h) Szemes, F.; Hesek, D.; Chen, Z.; Dent, S. W.; Drew, M. G. B.; Goulden, A. J.; Graydon, A. R.; Grieve, A.; Mortimer, R. J.; Wear, T.; Weightman, J. S.; Beer, P. D. *Inorg. Chem*. **1996**, *35*, 5868.

(6) (a) Hof, F.; Craig, S. L.; Nuckolls, C.; Rebek, J., Jr. *Angew. Chem., Int. Ed*. **2002**, *41*, 1488. (b) Beer, P. D.; Gale, P. A. *Angew. Chem., Int. Ed*. **2001**, *40*, 487. (c) Fleming, J. S.; Mann, K. L. V.; Carraz, C.-A.; Psillakis, E.; Jeffery, J. C.; McCleverty, J. A.; Ward, M. D. *Angew. Chem., Int. Ed*. **1998**, *37*, 1279. (d) Fujita, M.; Oguro, D.; Miyazawa, M.; Oka, H.; Yamaguchi, K.; Ogura, K. *Nature* **1995**, *378*, 469. (e) Kusukawa, T.; Fujita, M. *J. Am. Chem. Soc*. **1999**, *121*, 1397. (f) Hiraoka, S.; Fujita, M. *J. Am. Chem. Soc*. **1999**, *121*, 10239. (g) Kusukawa, T.; Yoshizawa, M.; Fujita, M. *Angew. Chem., Int. Ed*. **2001**, *40*, 1879. (h) Ibukuro, F.; Kusukawa, T.; Fujita M. *J. Am. Chem. Soc*. **1998**, *120*, 8561. (i) Vilar, R.; Mingos, D. M. P.; White, A. J. P.; Williams, D. J. *Angew. Chem., Int. Ed*. **1998**, *37*, 1258. (f) Navarro, J. A. R.; Janik, M. B. L.; Freisinger, E.; Lippert, B. *Inorg. Chem*. **1999**, *38*, 426. (g) Galindo, M. A.; Navarro, J. A. R.; Romero, M. A.; Quirós, M. *Dalton Trans*. **2004**, 1563.

(7) Barea, E.; Navarro, J. A. R.; Salas, J. M.; Quiróa, M.; Willermann, M.; Lippert, B. *Chem.—Eur. J*. **2003**, *9*, 4414.

(8) (a) Scherer, M.; Caulder, D. L.; Johnson, D. W.; Raymond, K. N. *Angew. Chem., Int. Ed*. **1999**, *38*, 1588. (b) McMorran, D. A.; Steel, P. J. *Angew. Chem., Int. Ed*. **1998**, *37*, 3295. (c) Su, Ch-Y.; Cai, Y-P.; Chen, C-L.; Lissner, F.; Kang, B-S.; Kaim, W. *Angew. Chem., Int. Ed*. **2002**, *41*, 3371. (d) Ruben, M.; Rojo, J.; Romero-Salguero, F. J.; Uppadine, L. H.; Lehn, J.-M. *Angew. Chem., Int. Ed*. **2004**, *43*, 3644.

(9) (a) Andruh, M. In *Encyclopedia of Supramolecular Chemistry*; Atwood, J. L., Steed, J. W., Eds.; Marcel Dekker, Inc.: New York, 2004; pp 1186−1193. (b) Ruben, M.; Breuning, E.; Lehn, J.-M.; Ksenofontov, V.; Renz, F.; Gütlich, P.; Vaughan, B. M. *Chem.—Eur. J*. **2003**, *9*, 4422. (c) Waldmann, O.; Hassmann, J.; Müller, P.; Hanan, G. S.; Volkmer, D.; Schubert, U. S.; Lehn, J.-M. *Phys. Rev. Lett*. **1997**, *78*, 3390.

(10) (a) Rojo, J.; Romero-Salguero, F. J.; Lehn, J.-M.; Baum, G.; Fenske, D. *Eur. J. Inorg. Chem*. **1999**, 1421. (b) Waldmann, O.; Ruben, M.; Zeiner, U.; Lehn, J.-M. *Inorg. Chem*. **2006**, *45*, 6535. (c) Waldmann, O.; Hassmann, J.; Müller, P.; Volkmer, D.; Schubert, U. S.; Lehn J.-M., *Phys. Rev. B* **1998**, *58*, 3277. (d) Milway, V. A.; Abedin, S. M. T.; Niel, V.; Nelly, T. L.; Dawe, L. N.; Dey, S. K.; Thompson, D. W.; Miller, D. O.; Alam, M. S.; Müller, P.; Thompson, L. K. *Dalton Trans*. **2006**, 2835.

(11) Ruben, M.; Lehn, J.-M., Müller, P. *Chem. Soc. Rev*. **2006**, *35*, 1056.

(12) Stadler, A.-M.; Kyritsakas, N.; Graff, R.; Lehn, J.-M. *Chem.—Eur. J*. **2006**, *12*, 4503.

(13) (a) Campos-Fernández, C. S.; Clérac, R.; Dunbar, K. R. *Angew. Chem., Int. Ed*. **1999**, *38*, 3477. (b) Ziessel, R.; Charbonnière, L.; Cesario, M.; Prangé, T.; Nierengarten, H. *Angew. Chem., Int. Ed*. **2002**, *41*, 975.

(14) Toyota, S.; Woods, C. R.; Benaglia, M.; Haldimann, R.; Wärnmark, K.; Hardcastle, K.; Siegel, J. S. *Angew. Chem., Int. Ed*. **2001**, *40*, 751.

(15) (a) Baxter, N. W.; Lehn, J.-M.; Kneisel, B. O.; Fenske, D. *Chem. Commun*. **1997**, 2231. (b) Ziessel, R.; Charbonnière, L.; Cesario, M.; Prangé, T.; Nierengarten, H. *Angew. Chem., Int. Ed*. **2002**, *41*, 975.

(16) Youinou, M.-T.; Rahmouni, N.; Fisher, J.; Osborn, J. A. *Angew. Chem., Int. Ed*. **1992**, *31*, 733.

(17) (a) Weissbuch, I.; Baxter, P. N. W.; Kuzmenko, I.; Cohen, H.; Cohen, S.; Kjaer, K.; Howes, P. B.; Als-Nielsen, J.; Lehn, J.-M. *Chem.—Eur. J*. **2000**, *6*, 725. (b) Baxter, P. N. W.; Lehn, J.-M.; Baum, G.; Fenske, D. *Chem.—Eur. J*. **2000**, *6*, 24. (c) Baxter, P. N. W.; Lehn, J.-M.; Kneisel, B. O.; Fenske, D. *Angew. Chem., Int. Ed*. **1997**, *36*, 1978. (d) Marquis, A.; Kintzinger, J.-P.; Graff, R.; Baxter, P. N. W.; Lehn, J.-M. *Angew. Chem., Int. Ed*. **2002**, *41*, 2760. (e) Baxter, P. N. W.; Lehn, J.-M.; Fischer, J.; Youinou, M.-T. *Angew. Chem., Int. Ed*. **1994**, *33*, 2284. (f) Weissbuch, I.; Baxter, P. N. W.; Cohen, S.; Cohen, H.; Kjaer, K.; Howes, P. B.; Als-Nielsen, J.; Hanan, G. S.; Schubert, U. S.; Lehn, J.-M.; Leiserowitz, L.; Lahav, M. *J. Am. Chem. Soc*. **1998**, *120*, 4850. (g) Baxter, P. N. W.; Lehn, J.-M.; Baum, G.; Fenske, D. *Chem.—Eur. J*. **2000**, *6*, 4510. (h) Brooker, S.; Davidson, T. C.; Hay, S. J.; Kelly, R. J.; Kennepohl, D. K.; Plieger, P. G.; Moubaraki, B.; Murray, K. S.; Bill, E.; Bothe, E. *Coord. Chem. Rev*. **2001**, *216−217*, 3.

(18) (a) Lan, Y.; Kennepohl, D. K.; Moubaraki, B.; Murray, K. S.; Cashion, J. D.; Jameson, G. B.; Broker, S. *Chem.—Eur. J*. **2003**, *9*, 3772. (b) Brooker, S.; Hay, S. J.; Plieger, P. G. *Angew. Chem., Int. Ed*. **2000**, *39*, 1968.

(19) (a) Salditt, T.; An, Q.; Plech, A.; Eschbaumer, C.; Schubert, U. S. *Chem. Commun*. **1998**, 2731. (b) Bassani, D. M.; Lehn, J.-M.; Fromm, K.; Fenske, D. *Angew. Chem., Int. Ed*. **1998**, *37*, 2364. (c) Ruben, M.; Breuning, E.; Gisselbrecht, J.-P.; Lehn, J.-M. *Angew. Chem., Int. Ed*. **2000**, *39*, 4139. (d) Uppadine, L. H.; Lehn, J.-M. *Angew. Chem., Int. Ed*. **2004**, *43*, 240. (e) Hanan, G. S.; Volkmer, D.; Schubert, U. S.; Lehn, J.-M.; Baum, G.; Fenske, D. *Angew. Chem., Int. Ed*. **1997**, *36*, 1842.

(20) (a) Duan, C.-Y.; Liu, Z.-H.; You, X.-Z.; Xue, F.; Mak, T. C. W. *Chem. Commun*. **1997**, 381. (b) Bark, T.; Düggeli, M.; Stoeckli-Evans, H.; von Zelewsky, A. *Angew. Chem., Int. Ed*. **2001**, *40*, 2848.

(21) (a) Mann, K. L. V.; Psillakis, E.; Jeffery, J. C.; Rees, L. H.; Harden, N. M.; McCleverty, J. A.; Ward, M. D.; Gatteschi, D.; Totti, F.; Mabbs, F. E.; McInnes, E. J. L.; Riedi, P. C.; Smith, G. M. *J. Chem. Soc., Dalton Trans*. **1999**, 339. (b) Rojo, J.; Lehn, J-M.; Baum, G.; Fenske, D.; Waldmann, O.; Müller, P. *Eur. J. Inorg. Chem*. **1999**, 517.

(22) Helgeson, R. C.; Lauer, M.; Cram, D. J. *J. Chem. Soc. Chem. Commun*. **1983**, 101.

Chart 1

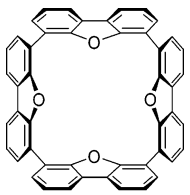

Cram's cavitand

Chart 2

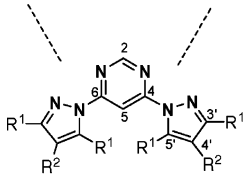

$R^1 = R^2 = H$ (bpzpm)
$R^1 = Me$, $R^2 = H$ (bpz*pm)
$R^1 = H$, $R^2 = Me$ (Mebpzpm)

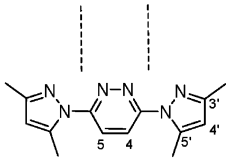

ppdMe

stacked with the dibenzofurane units.[23] These macrocyclic structures were obtained in low yields (ca. 11%) by complicated synthetic procedures. The inorganic counterparts could imply a much more simple preparation on the basis of the self-recognition of the organic and metallic components. To achieve this goal, we designed and synthesized a series of ligands containing two pyrazolyl groups bonded to a central pyrimidine ring in 4 and 6 positions: 4,6-bis(pyrazol-1-yl)pyrimidine (bpzpm), 4,6-bis(3,5-dimethylpyrazol-1-yl)pyrimidine (bpz*pm), and 4,6-bis(4-methylpyrazol-1-yl)pyrimidine (Mebpzpm) (Chart 2). These ditopic ligands exhibit a quasirigid, planar structure and are obviously able to coordinate two CuL_2 units in a chelating way. Because of the disposition of the nitrogen atoms in the central rings, the ligands when coordinated should adopt a cisoid conformation. The dotted lines represent the binding vectors and constitute the projection of the planes where the Cu(I) centers and the ligands that complete the coordination sphere should be situated. The reaction of these ligands with bare Cu(I) centers should lead to the targeted metallic grids. We thought that the cavities generated in these grids would be able to host anionic guests such as their own counteranions. One point that could favor this encapsulation could be the existence of anion$-\pi$ interactions with the π-acidic ring of pyrimidine. These types of interactions[24] have recently received considerable attention, and they have been found not only with anions as simple as halides but also with multiatomic anions. The π-acidic systems studied include substituted benzenes,[24e] aromatic rings with acidity enhanced by its union to metal centers,[24c,g,h] and also heterocycles such as *s*-triazines,[24a,b,d,i] pyridazine,[24i] tetrazine,[24i] and pyrazine[24f] rings. We will show in this work the validity of this hypothesis with different anions, and we will show that anion$-\pi$ interactions involving the pyrimidine and pyridazine rings are possible. The choice of differently substituted pyrazolyl rings was made with the aim of evaluating the effect produced by changes in the electronic or steric properties of the coordinated rings. Although ligands containing pyrimidine rings are frequently used in the formation of grids, they are clearly different from those proposed here. They may be considered of the type, bis(tridentade), and they give rise to [2 × 2] grids with parallel ligands after reaction with octahedral metals.[7,9,10,19] There has been described a case of grids with tetrahedral centers and a ligand of the type 4,6-bis(pyrid-2-yl)pyrimidine, but in this case, the facing ligands are nearly parallel.[25] On the other hand, the use of pyrazolyl rings in the ligands has been until now very scarcely explored in the formation of metallic grids.[21]

We also decided to obtain a ligand containing similar pyrazole fragments but with a disposition that would lead to parallel binding vectors. To get this geometry, the central ring chosen was a pyridazine heterocycle substituted in the 3 and 6 positions, 3,6-bis(3,5-dimethylpyrazol-1-yl)pyridazine (ppdMe, Chart 2). In this way, the influence of the relative disposition of the binding vectors in the ligand over the type of grid obtained could be clearly evaluated. Besides, as a result of the different relative disposition of the nitrogen atoms in the central ring and their distance, we should obtain grids of different cavity sizes with both types of ligands. The use of ligands containing pyridazine as the central ring has been already explored but usually bonded to six-membered rings like pyridine[26] or those belonging to a macrocycle[17h] but never to five-membered rings like pyrazole.

To obtain complementary information about the new derivatives, besides other more-conventional structural techniques, we have also used NMR diffusion spectroscopy. Recently, attention has focused increasingly on the solution characterization of supramolecular entities with this methodology.[27] The diffusion coefficients are sensitive to structural properties of the observed species such as weight, size, and shape and also to binding processes and molecular interactions. Diffusion experiments were used recently to probe the structure of a dodecahedron constructed from 50 predesigned components and some rotaxanes.[28] Hydrogen-bonded rosettes or helical organizations, double−strand

(23) Schwartz, E. B.; Knobler, C. B.; Cram, D. J. *J. Am. Chem. Soc.* **1992**, *114*, 10775.

(24) (a) Mascal, M.; Armstrong, A.; Bartberger, M. D. *J. Am. Chem. Soc.* **2002**, *124*, 6274. (b) Demeshko, S.; Dechert, S.; Meyer, F. *J. Am. Chem. Soc.* **2004**, *126*, 4508. (c) Fairchild, R. M.; Holman, K. T. *J. Am. Chem. Soc.* **2005**, *127*, 16364. (d) Frontera, A.; Saczewski, F.; Gdaniec, M.; Dziemidowicz-Borys, E.; Kurland, A.; Deyà, P. M.; Quiñonero, D.; Garau, C. *Chem.—Eur. J.* **2005**, *11*, 6560 and references therein. (e) Frontera, A.; Quiñonero, D.; Costa, A.; Ballester, P.; Deyà, P. M. *New. J. Chem.* **2007**, *31*, 556. (f) Black, C. A.; Hanton, L. R.; Spicer, M. D. *Inorg. Chem.* **2007**, *46*, 3669. (g) Holman, K. T.; Halihan, M. M.; Jurisson, S. S.; Atwood, J. L.; Burkhalter, R. S.; Mitchell, A. R.; Steed, J. W. *J. Am. Chem. Soc.* **1996**, *118*, 9567. (h) Staffilani, M.; Hancock, K. S. B.; Steed, J. W.; Holman, K. T.; Atwood, J. L.; Juneja, R. K.; Burkhalter, R. S. *J. Am. Chem. Soc.* **1997**, *119*, 6324. (i) Schottel, B. L.; Chifotides, H. T.; Shatruck, M.; Chouai, A.; Pérez, L. M.; Bacsa, J.; Dunbar, K. R. *J. Am. Chem. Soc.* **2006**, *128*, 5895.

(25) Patroniak, V.; Stefankiewicz, A. R.; Lehn, J.-M.; Kubicki, M. *Eur. J. Inorg. Chem.* **2005**, 4168.

(26) Hoogenboom, R.; Kickelbick, G.; Schubert, U. S. *Eur. J. Org. Chem.* **2003**, 4887.

(27) (a) Price, W. *Concepts Magn. Reson.* **1997**, *9*, 299. (b) Price, W. *Concepts Magn. Reson.* **1998**, *10*, 197. (c) Johnson, C. S., Jr. *Prog. Nucl. Magn. Reson.* **1999**, *34*, 203. (d) Cohen, Y.; Avram, L.; Frish, L. *Angew. Chem., Int. Ed.* **2005**, *44*, 520.

helicates, and polygon assemblies were also characterized in solution with these techniques,[29] as have ion-pairing interactions in organometallic systems.[30]

Experimental Section

General Comments. All of the manipulations were carried out under an atmosphere of dry oxygen-free nitrogen using standard Schlenk techniques. Solvents were distilled from the appropriate drying agents and degassed before use. Elemental analyses were performed with a Thermo Quest FlashEA 1112 microanalyzer. IR spectra were recorded as KBr pellets or Nujol mulls with a PerkinElmer PE 883 IR or a Jasco FTIR-6300 type-A spectrometers. FAB^+ MS measurements were made with a VG BIOTECH QUATTRO spectrometer. ^1H, $^{13}C\{^1H\}$, ^{19}F and, $^{31}P\{^1H\}$ NMR spectra were recorded on a Varian Unity 300, a Varian Gemini 400, and an Inova 500 spectrometer. Chemical shifts (ppm) are relative to TMS (^1H, ^{13}C NMR), $CFCl_3$ (^{19}F-NMR), and 85% H_3PO_4 (^{31}P NMR). Coupling constants (*J*) are in Hertz. The NOE difference spectra were recorded with a 5000 Hz spectrum width, acquisition time 3.27 s, pulse width 90°, relaxation delay 4 s, irradiation power 5−10 dB, number of scans 240. For ^1H-^{13}C, *g*-HSQC, and *g*-HMQC spectra, the standard VARIAN pulse sequences were used (VNMR 6.1 C software). The spectra were acquired using 7996 (^1H) and 25133.5 Hz (^{13}C) spectrum widths; 16 transients of 2048 data points were collected for each of the 256 increments. For variable temperature spectra, the probe temperature (±1 K) was controlled by a standard unit calibrated with a methanol reference. In the NMR data, s, d, and b refer to singlet, doublet, and broad, respectively. The carbon resonances are singlets. Resonances marked with ″ belong to the *p*-$CH_3-C_6H_4-SO_3$ counteranion. Diffusion NMR measurements were carried out with a Bruker DRX500 using the BPP-LED sequence,[31] with sample temperatures regulated at 298 K. A Bruker triple-resonance inverse probehead was employed on which the nominal ^1H channel could also be tuned down to ^{19}F, allowing measurements on both nuclei. Sample spinning at 20 Hz was employed to eliminate convection interference[32] with diffusion periods ($\Delta = 50$ ms) selected to ensure integer tube revolutions during this time. Diffusion encoding gradients were set to 4 ms total duration (δ) and were applied as bipolar pairs[33] with typically 8−16 gradient increments employed to map the diffusion behavior. Data were analyzed with either the curve-fitting routines provided in Bruker's XWINNMR software or with fitting routines within suitable Microsoft Excel spreadsheets using the Solver tool. The ligands bpzpm,[34] bpz*pm,[35] and Mebpzpm[36] were prepared as previously described. Although the ligand ppdMe was first described by Elguero et al.,[37] we used a different method for its synthesis, similar to that described by Thompson et al.[38] but using NaH instead of K to deprotonate the pyrazolyl ring. $[Cu(CH_3CN)_4]X$, X = PF_6, BF_4, ClO_4 were prepared according to the literature.[39]

Syntheses of the New Derivatives. $[Cu(bpzpm)]_nCl_n$, 1. A suspension of 28.0 mg (0.283 mmol) of CuCl in 10 mL of acetone was added to a solution of 60.0 mg (0.283 mmol) of bpzpm in 10 mL of acetone. Immediately, a brown suspension was formed that was stirred at room temperature for 1 h. After this time, it was concentrated up to 5 mL, and the brown solid of **1** was filtrated and dried. The product was crystallized from CH_2Cl_2/hexane, and a microcrystalline product was obtained. Yield 64.2 mg (73%). Anal. Calcd for **1·CH_2Cl_2**: C, 37.03; H, 2.58; N, 25.28. Found: C, 37.26; H, 2.78; N, 25.03. ^1H NMR ($CDCl_3$, 300 MHz, 25 °C): $\delta = 8.78$ (bs, 1H, H^2), 8.56 (bs, 2H, $H^{5'}$), 8.43 (bs, 1H, H^5), 7.80 (bs, 2H, $H^{3'}$), 6.51 (bs, 2H, $H^{4'}$). ^1H NMR ($CDCl_3$, 300 MHz, −60 °C): $\delta = 8.81$ (s, 1H, H^2), 8.59 (s, 2H, $H^{5'}$), 8.46 (s, 1H, H^5), 7.85 (s, 2H, $H^{3'}$), 6.56 (s, 2H, $H^{4'}$) ppm. IR (Nujol) ν/cm^{-1} 1608 (ν(C═N)), 227 (ν(Cu−Cl)). MS (FAB^+, NBA): *m*/*z* (rel. int. %): 1013 [M^+-bpzpm-PF_6, 0.3], 949 [M^+-Cu-bpzpm-PF_6, 0.4], 836 [M^+-2Cu-bpzpm-2PF_6, 0.9], 802 [M^+-2Cu-bpzpm-3PF_6, 0.9], 487 [M^+-3Cu-2bpzpm-4PF_6, 40.6], 307 [M^+-3Cu-3bpzpm-3PF_6, 79.2], 275 [M^+-3Cu-3bpzpm-3PF_6, 77.0], 213 [M^+-4Cu-3bpzpm-4PF_6, 100.0] D.

$[Cu(bpzpm)]_4(PF_6)_4$, 2. A solution of 100.0 mg (0.268 mmol) of $[Cu(CH_3CN)_4]PF_6$ in 20 mL of CH_2Cl_2 was added to a solution of 56.9 mg (0.268 mmol) of bpzpm in 10 mL of CH_2Cl_2. An orange precipitate appeared instantaneously. The suspension was stirred at room temperature for 1 h and was then filtered. The obtained orange solid was dried under a vacuum. Yield 107.1 mg (95%). Anal. Calcd for **2**: C, 28.55; H, 1.92; N, 19.98. Found: C, 28.31; H, 1.77; N, 19.73. ^1H NMR (acetone-d_6, 400 MHz, 25 °C): $\delta =$ 9.04 (d, 2H, $J_{4'-5'} = 2.9$ Hz, $H^{5'}$), 8.88 (s, 1H, H^2), 8.80 (s, 1H, H^5), 8.19 (d, 2H, $J_{3'-4'} = 1.8$ Hz, $H^{3'}$), 7.06 (dd, 2H, $H^{4'}$) ppm. ^{19}F NMR (acetone-d_6, 300 MHz, 25 °C): $\delta = -75.0$ (d, $J = 708$) ppm. IR (Nujol) ν/cm^{-1} 1602 (ν(C═N)), 839 (ν(P−F)), 555 (δ-(P−F)). MS (FAB^+, NBA): *m*/*z* (rel. int. %): 1537 [M^+-PF_6, 3], 487 [M^+-4PF_6-3Cu−2bpzpm, 100] D.

$[Cu(bpzpm)]_4(BF_4)_4$, 3. The synthesis of **3** is similar to that of **2**. The amounts of products were as follows: 89.0 mg (0.283 mmol) of $[Cu(CH_3CN)_4]BF_4$ and 60.0 mg (0.283 mmol) of bpzpm. **3** is red in color. Yield 85.1 mg (83%). Crystals of **3** were obtained by diffusion of the starting reagents using three phases. The lower phase was $[Cu(CH_3CN)_4]BF_4$ solved in dichloromethane, a phase of acetone was put in the middle, and the upper phase contained bpzpm solved in diethyl ether. Anal. Calcd for **3·2C_3H_6O·CH_2Cl_2.** C, 34.19; H, 2.81; N, 20.36. Found: C, 34.54; H, 2.80; N, 20.37. ^1H NMR (acetone-d_6, 400 MHz, 25 °C): $\delta = 9.06$ (bs, 1H, H^2), 9.04 (d, 2H, $J_{4'-5'} = 2.9$ Hz, $H^{5'}$), 8.78 (bs, 1H, H^5), 8.21 (bs, 2H, $H^{3'}$), 7.05 (bs, 2H, $H^{4'}$) ppm. ^{19}F NMR (acetone-d_6, 300 MHz, 25 °C): $\delta = -154.4$ ppm. IR (Nujol) ν/cm^{-1} 1601 (ν(C═N)), 1074, 1049 (ν(B−F)), 533 (δ(B−F)). MS (FAB^+, NBA): *m*/*z* (rel. int.

(28) (a) Olenyuk, B.; Levin, M. D.; Whiteford, J. A.; Shield, J. E.; Stang, P. J. *J. Am. Chem. Soc.* **1999**, *121*, 10434. (b) Skinner, P. J.; Blair, S.; Kataky, R.; Parker, D. *New. J. Chem.* **2000**, *24*, 265.

(29) (a) Timmerman, P.; Weidmann, J.-L.; Jolliffe, K. A.; Prins, L. J.; Reinhoudt, D. N.; Shinkai, S.; Frish, L.; Cohen, Y. *J. Chem. Soc., Perkin Trans.* **2000**, *2*, 2077, (b) Barberá, J.; Puig, L.; Romero, P.; Serrano, J. L.; Sierra, T. *J. Am. Chem. Soc.* **2006**, *128*, 4487. (c) Allouche, L.; Marquis, A.; Lehn, J.-M. *Chem.—Eur. J.* **2006**, *12*, 7520. (d) Otto, W. H.; Keefe, M. H.; Splan, K. E.; Hupp, J. T.; Larive, C. K. *Inorg. Chem.* **2002**, *41*, 6172. (e) Megyes, T.; Jude, H.; Grósz, T.; Bakó, I.; Radnai, T.; Tárkányi, G.; Pálinkás, G.; Stang, P. J. *J. Am. Chem. Soc.* **2005**, *127*, 10731.

(30) (a) Pregosin, P. S.; Martínez-Viviente, E.; Kumar, A. *Dalton Trans.* **2004**, 4007. (b) Pregosin, P. S.; Kumar, P. G. A.; Fernandez, I. *Chem. Rev.* **2005**, *105*, 2977.

(31) Wu, D.; Chen, A.; Johnson, C. S. *J. Magn. Reson. Ser. A* **1995**, *115*, 260.

(32) Esturau, N.; Sánchez-Ferrando, F.; Gavin, J. A.; Roumestand, C.; Delsuc, M.-A.; Parella, T. *J. Magn. Reson.* **2001**, *153*, 48.

(33) Wider, G.; Dotsch, V.; Wuthrich, K. *J. Magn. Reson., Ser. A* **1994**, *108*, 255.

(34) Ikeda, M.; Maruyama, K.; Nobuhara, Y.; Yamada, T.; Okabe, S. S. *Chem. Pharm. Bull.* **1997**, *45*, 549.

(35) Usón, R.; Oro, L. A.; Esteban, M.; Carmona, D.; Claramunt, R. M.; Elguero, J. *Polyhedron* **1984**, *3*, 213.

(36) Gómez-de la Torre, F.; de la Hoz, A.; Jalón, F. A.; Manzano, B. R.; Rodríguez, A. M.; Elguero, J.; Martínez-Ripoll, M. *Inorg. Chem.* **2000**, *39*, 1152.

(37) Elguero, J.; Jacquier, R.; Mondon, S. *Bull. Soc. Chim. Fr.* **1970**, 1346.

(38) Thompson, L. K.; Woon, T. C.; Murphy, D. B.; Gabe, E. J.; Lee, F. L.; Le Page, Y. *Inorg. Chem.* **1985**, *24*, 4719.

(39) Kubas, G. J. *Inorg. Synth.* **1979**, *19*, 90.

%): 1363 [M^+-BF_4, 0.4], 1215 [M^+-Cu-2BF_4, 0.2], 1081 [M^+-Cu-bpzpm-BF_4, 0.4], 1001 [M^+-Cu-bpzpm-2BF_4, 0.3], 803 [M^+-2Cu-2bpzpm-BF_4, 1.0], 576 [M^+-3Cu-2bpzpm-3BF_4, 4.9], 487 [M^+-3Cu-2bpzpm-4BF_4, 36.3], 275 [M^+-3Cu-3bpzpm-4BF_4, 100.0] D.

[Cu(bpzpm)]$_4$(ClO_4)$_4$, 4. The synthesis of **4** is similar to that of **2**. The amounts of products were as follows: 77.1 mg (0.236 mmol) of [Cu(CH_3CN)$_4$]ClO_4 and 50.0 mg (0.236 mmol) of bpzpm. **4** is orange. Yield 82.2 mg (93%). It was crystallized by diffusion of the starting reagents in a mixture of dichloromethane plus [Cu(CH_3CN)$_4$]ClO_4)/acetone/diethyl ether plus bpzpm. Anal. Calcd for **4·2CH_2Cl_2**: C, 30.20; H, 2.17; N, 20.12. Found: C, 30.48; H, 2.14; N, 20.36. ^{1}H NMR (acetone-d_6, 400 MHz, 25 °C): δ = 9.06 (bs, 1H, H^2), 9.04 (bs, 2H, $H^{5'}$), 8.78 (bs, 1H, H^5), 8.21 (bs, 2H, $H^{3'}$), 7.05 (bs, 2H, $H^{4'}$) ppm. ^{1}H NMR ($CDCl_3$, 300 MHz, 25 °C): δ = 8.80 (bs, 1H, H^2), 8.60 (bs, 2H, $H^{5'}$), 8.49 (bs, 1H, H^5), 7.86 (bs, 2H, $H^{3'}$), 6.53 (bs, 2H, $H^{4'}$) ppm. IR (Nujol) ν/cm^{-1} 1604 (ν(C═N)), 1103 (ν(Cl−O)), 623 (δ(Cl−O)). MS (FAB$^+$, NBA): *m*/*z* (rel. int. %): 1237 [M^+-Cu− 2ClO_4, 1.9], 1090 [M^+-bpzpm-2ClO_4, 1.6], 1025 [M^+-Cu-bpzpm-2ClO_4, 2.5], 813 [M^+-Cu-2bpzpm-2ClO_4, 3.0], 677 [M^+-2bpzpm-4ClO_4, 3.5], 649 [M^+- 2Cu-2bpzpm-3ClO_4, 6.5], 487 [M^+-3Cu-2bpzpm- 4ClO_4, 41.2], 275 [M^+-3Cu-3bpzpm-4ClO_4, 100.0] D.

[Cu(bpzpm)]$_4$(CF_3SO_3)$_4$, 5. To a suspension of 88.4 mg of [Cu(bpzpm)]$_n$(Cl)$_n$ (**1**) in 30 mL of acetone, 72.7 mg (0.283 mmol) of Ag(CF_3SO_3) were added. The brown suspension turned instantaneously into an orange suspension that was stirred at room temperature for 7 h, protected from light. After that, the insoluble AgCl was filtered off. The solution was evaporated until it was dry under a vacuum, and an orange solid was obtained that was washed with THF. Yield 68.8 g (57%). Anal. Calcd for **5**: C, 32.12; H, 2.18; N, 19.13; S, 7.30. Found: C, 31.74; H, 2.56; N, 19.46; S, 6.93. ^{1}H NMR (acetone-d_6, 400 MHz, 25 °C): δ = 9.11 (bs, 1H, H^2), 9.09 (bs, 2H, $H^{5'}$), 8.85 (s, 1H, H^5), 8.18 (bs, 2H, $H^{3'}$), 7.03 (bs, 2H, $H^{4'}$). ^{19}F NMR (acetone-d_6, 300 MHz, 25 °C): δ = −77.2 (s). IR (Nujol) ν/cm^{-1} 1605 (ν(C═N)), 1261, 1156, 1124, 638 (CF_3-SO_3). MS (FAB$^+$, NBA): *m*/*z* (rel. int. %): 1549 [M^+-CF_3SO_3, 0.1], 1337 [M^+-Cu-2CF_3SO_3, 0.1], 1251 [M^+-3CF_3SO_3, 0.1], 1210 [M^+-Cu-2bpzpm , 0.3], 1062 [M^+-Cu-2bpzpm-CF_3SO_3, 0.6], 1039 [M^+-bpzpm-3CF_3SO_3, 0.2], 999 [M^+-2Cu-2bpzpm-CF_3SO_3, 1.6], 699 [M^+-2Cu-2bpzpm-3CF_3SO_3, 2.2], 636 [M^+-3Cu-2bpzpm-3 CF_3-SO_3, 3.8], 487 [M^+-3Cu-2bpzpm-4CF_3SO_3, 73.1], 424 [M^+-3Cu-3bpzpm-3 CF_3SO_3, 30.2], 275 [M^+-3Cu-3bpzpm-4CF_3SO_3, 100.0] D.

[Cu(bpzpm)]$_4$(*p*-CH_3−C_6H_4−SO_3)$_4$, 6. The synthesis of **6** is similar to that of **5**. The amounts were as follows: 88.4 mg of [Cu(bpzpm)]$_n$(Cl)$_n$ and 78.9 mg (0.283 mmol) of Ag(*p*-CH_3−C_6H_4−SO_3). **6** is orange in color. Yield 77.1 mg (61%). Anal. Calcd for **6·C_3H_6O**: C, 46.20; H, 3.60; N, 18.21; S, 6.95. Found: C, 46.04; H, 3.76; N, 18.98; S, 6.53. IR (Nujol) ν/cm^{-1} 1603 (ν(C═N)), 1218, 1189, 1032, 1010, 816, 680, 565 (*p*-CH_3−C_6H_4−SO_3). MS (FAB$^+$, NBA): *m*/*z* (rel. int. %): 1191 [M^+-2bpzpm-$C_7H_7SO_3$, 0.1], 1065 [M^+-2Cu-2bpzpm-3$C_7H_7SO_3$, 0.4], 1061 [M^+- bpzpm-3$C_7H_7SO_3$, 0.3], 807 [M^+-3bpzpm-2$C_7H_7SO_3$, 0.7], 745 [M^+-Cu-3bpzpm-2 $C_7H_7SO_3$, 1.5], 680 [M^+-2Cu-3bpzpm-2$C_7H_7SO_3$, 2.5], 509 [M^+-2Cu-3bpzpm-3$C_7H_7SO_3$, 46.2], 487 [M^+-3Cu-2bpzpm-4$C_7H_7SO_3$, 26.1], 446 [M^+-3Cu-3bpzpm-3 $C_7H_7SO_3$, 20.9], 275 [M^+-3Cu-3bpzpm-4$C_7H_7SO_3$, 100.0] D.

[Cu(bpz*pm)]$_n$(Cl)$_n$, 7. The synthesis of **7** is similar to that of **1** with the ligand bpz*pm. The amounts were as follows: 22.2 mg (0.224 mmol) of CuCl and 60.0 mg (0.224 mmol) of bpz*pm. In this case, a pale-pink suspension was formed. **7** is pale orange in color. The complex was recrystallized from dichloromethane/pentane. Yield 60.8 mg (74%). Anal. Calcd for **7·1/2CH_2Cl_2**: C, 44.89; H, 4.33; N, 22.24. Found: C, 44.94; H, 4.54; N, 22.04. ^{1}H NMR ($CDCl_3$, 300 MHz, −60 °C): δ = 8.89 (s, 1H, H^2), 8.12 (s, 1H, H^5), 6.17 (s, 2H, $H^{4'}$), 2.73 (s, 6H, $Me^{5'}$), 2.34 (s, 6H, $Me^{3'}$) ppm. IR (Nujol) ν/cm^{-1} 1600 (ν(C═N)), 239 (ν(Cu−Cl)). UV−vis (CH_2Cl_2) λ (ϵ): 260 (1.00 × 10^5), 295 (1.22 × 10^5) nm. MS (FAB$^+$, NBA): *m*/*z* (rel. int. %): 1401 [M^+-2Cl, 0.5], 1267 [M^+-2Cu-2Cl, 1.8], 931 [M^+-2Cu-bpz*pm-4Cl, 4], 634 [M^+-3Cu-2bpz*pm-3Cl, 9.35]$^+$, 564 [M^+-Cu-3bpz*pm-Cl, 28.0], 557 [M^+-3bpz*pm-3Cl, 50.7], 494 [M^+-Cu-3bpz*pm-3Cl, 8.9], 431 [M^+-Cu-3bpz*pm-3Cl, 16.3], 331 [M^+-3Cu-3bpz*pm-4Cl, 100.0] D.

[Cu(bpz*pm)]$_4$(PF_6)$_4$, 8. A solution of 100.0 mg (0.268 mmol) of [Cu(CH_3CN)$_4$](PF_6) in 20 mL of CH_2Cl_2 was added a solution of 72.0 mg (0.268 mmol) of bpz*pm in 10 mL of CH_2Cl_2. A red suspension was formed that was stirred at room temperature during 1 h, concentrated, and filtrated. The red solid obtained was dried under a vacuum. Yield 104.5 mg (82%). Anal. Calcd for **8**: C, 35.27; H, 3.38; N, 17.62. Found: C, 35.17; H, 3.47; N, 17.34. ^{1}H NMR (acetone-d_6, 400 MHz, 25 °C): δ = 8.78 (s, 1H, H^2), 8.14 (s, 1H, H^5), 6.63 (s, 2H, $H^{4'}$), 2.95 (s, 6H, $Me^{5'}$), 2.21 (s, 6H, $Me^{3'}$) ppm. ^{19}F NMR (acetone-d_6, 300 MHz, 25 °C): δ = −74.5 (d, J = 721 Hz). IR (Nujol) ν/cm^{-1} 1602(ν(C═N)), 839 (ν(P−F)), 559 (δ-(P−F)). UV−vis (CH_2Cl_2) λ (ϵ): 298 (1.40 × 10^5), 407 (1.96 × 10^4) nm.

[Cu(bpz*pm)]$_4$(BF_4)$_4$, 9. The synthesis of **9** is similar to that of **8**. The amounts were as follows: 55.0 mg (0.175 mmol) of [Cu(CH_3CN)$_4$](BF_4) and 47.0 mg (0.175 mmol) of the ligand bpz*pm. Yield 92.3 mg (98%). The red solid was recrystallized from a mixture of 1,2-dicloroethane/hexane. Anal. Calcd for **9·$C_2H_4Cl_2$**: C, 39.28; H, 3.86; N, 18.95. Found: C, 39.40; H, 3.84; N, 19.12. ^{1}H NMR (acetone-d_6, 400 MHz, 25 °C): δ = 8.94 (s, 1H, H^2), 8.14 (s, 1H, H^5), 6.62 (s, 2H, $H^{4'}$), 2.95 (s, 6H, $Me^{5'}$), 2.21 (s, 6H, $Me^{3'}$) ppm. ^{19}F NMR (acetone-d_6, 300 MHz, 25 °C): δ = −153.5 ppm. ^{13}C{^{1}H} NMR (acetone-d_6, 500 MHz, 25 °C): δ = 157.0 (s, 1C, C^2), 155.3 (s, 2C, $C^{4,6}$), 151.7 (s, 2C, $C^{3'}$), 144.2 (s, 2C, $C^{5'}$), 114.0 (s, 2C, $C^{4'}$), 96.8 (s, 1C, C^5), 14.4 (s, 2C, $Me^{5'}$), 13.8 (s, 2C, $Me^{3'}$) ppm. IR (Nujol) ν/cm^{-1} 1602(ν(C═N)), 1058, 1033 (ν(B−F)), 548 (δ(B−F)). UV−vis (CH_2Cl_2) λ (ϵ): 298 (1.23 × 10^5), 407 (1.87 × 10^4) nm. MS (FAB$^+$, NBA): *m*/*z* (rel. int. %): 1587 [M^+-BF_4, 0.6], 1398 [M^+-3Cu-BF_4, 0.3], 1250 [M^+-Cu bpz*pm-BF_4, 0.2], 1169 [M^+-Cu−bpz*pm-2BF_4, 1.0], 931 [M^+-2Cu−bpz*pm-4BF_4, 0.5], 868 [M^+-3Cu−bpz*pm-4BF_4, 1.2], 750 [M^+-2Cu-2bpz*pm-3BF_4, 2.5], 662 [M^+-2Cu-2bpz*pm-4BF_4, 2.5], 599 [M^+-3Cu-2bpz*pm-4BF_4, 20.9], 413 [M^+-3Cu-3bpz*pm-3BF_4, 67.5], 331 [M^+-3Cu-3bpz*pm-4BF_4, 100.0] D.

Synthesis of [Cu(bpz*pm)]$_4$(ClO_4)$_4$, 10. 10 has been synthesized in two ways:

Method a. It is analogous to that used for **8**. The amounts were as follows: 60.9 mg (0.186 mmol) of [Cu(CH_3CN)$_4$]ClO_4 and 50.0 mg (0.186 mmol) of the ligand bpz*pm. The complex was crystallized by diffusion of the reactants in a mixture of the following phases: dichloromethane plus [Cu(CH_3CN)$_4$]ClO_4/acetone/diethyl ether plus bpz*pm. **10** is orange in color. Yield 73.2 mg (91%). Anal. Calcd for **10**: C, 38.99; H, 3.74; N, 19.48. Found: C, 39.26; H, 3.83; N, 19.82. ^{1}H NMR (acetone-d_6, 400 MHz, 25 °C): δ = 8.88 (s, 1H, H^2), 8.12 (s, 1H, H^5), 6.61 (s, 2H, $H^{4'}$), 2.93 (s, 6H, $Me^{5'}$), 2.21 (s, 6H, $Me^{3'}$) ppm. ^{1}H NMR ($CDCl_3$, 400 MHz, 25 °C): δ 8.76 (s, 1H, H^2), 7.85 (s, 1H, H^5), 6.31 (s, 2H, $H^{4'}$), 2.77 (s, 6H, $Me^{5'}$), 2.21 (s, 6H, $Me^{3'}$) ppm. ^{13}C{^{1}H} NMR (acetone-d_6, 500 MHz, 25 °C): δ = 155.3 (s, 2C, $C^{4,6}$), 151.6 (s, 2C, $C^{3'}$), 144.2 (s, 2C, $C^{5'}$), 114.0 (s, 2C, $C^{4'}$), 97.0 (s, 1C, C^5), 14.5 (s, 2C, $Me^{5'}$), 13.9 (s, 2C, $Me^{3'}$) ppm. IR (Nujol) ν/cm^{-1} 1603-(ν(C═N)), 1092 (ν(Cl−O)), 623 (δ(Cl−O)). UV−vis (CH_2Cl_2) λ (ϵ): 298 (1.42 × 10^5), 407 (1.93 × 10^4) nm. MS (FAB$^+$, NBA):

m/*z* (rel. int. %): 1625 [M^+-ClO_4, 0.6], 331 [M^+-3Cu-3bpz*pm-4ClO_4, 100.0] D.

Method b. Complex [Cu(bpz*pm)]$_n$(Cl)$_n$·1/2CH_2Cl_2 (**7·1/2CH_2Cl_2**), 70.3 mg, and $AgClO_4$, 38.6 mg (0.186 mmol) were mixed in 30 mL of acetone. An orange suspension was formed that was stirred for 8 h. Then, AgCl was removed by filtration, the solution was evaporated to dryness, and the solid was washed with THF. Yield 44.9 mg (56%).

[Cu(bpz*pm)]$_4$(CF_3SO_3)$_4$, 11. The synthesis of the new orange complex **11** is analogous to that of **10**, using method b. The amounts were as follows: 84.5 mg of [Cu(bpz*pm)]$_n$Cl$_n$, **7**, and 57.5 mg (0.224 mmol) of Ag(CF_3SO_3). Complex **11** is orange-red colored. Yield 60.3 g (56%). Anal. Calcd for **11**: C, 34.77; H, 3.63; N, 13.24; S, 5.05. Found: C, 34.50; H, 4.01; N, 13.04; S, 5.20. ^{1}H NMR (acetone-d_6, 400 MHz, 25 °C): δ = 8.99 (s, 1H, H^2), 8.14 (s, 1H, H^5), 6.62 (s, 2H, H$^{4'}$), 2.94 (s, 6H, Me$^{5'}$), 2.22 (s, 6H, Me$^{3'}$) ppm. ^{19}F NMR (acetone-d_6, 300 MHz, 25 °C): δ = −80.0 ppm. ^{13}C{^{1}H} NMR (acetone-d_6, 500 MHz, 25 °C): δ = 156.9 (s, 2C, C^2),155.4 (s, 2C, C^{4,6}), 151.6 (s, 2C, C$^{3'}$), 144.1 (s, 2C, C$^{5'}$), 114.0 (s, 2C, C$^{4'}$), 96.9 (s, 1C, C^5), 14.6 (s, 2C, Me$^{5'}$), 13.8 (s, 2C, Me$^{3'}$) ppm. IR (Nujol) ν/cm^{-1} 1601(ν(C═N)), 1263, 1143, 1122, 637 (CF_3SO_3). UV−vis (CH_2Cl_2) λ (ϵ): 298 (1.04 ×× 10^5), 407 (1.40 × 10^4) nm. MS (FAB$^+$, NBA): *m*/*z* (rel. int. %): 1775 [M^+- CF_3SO_3, 0.2], 1323 [M^+-Cu-2bpz*pm, 0.2], 599 [M^+-3Cu-2bpz*pm-4 CF_3SO_3, 11.3], 331 [M^+-3Cu-3bpz*pm-4CF_3SO_3, 100.0] D.

[Cu(bpz*pm)]$_4$(*p*-CH_3−C_6H_4−SO_3)$_4$, 12. The synthesis of **12** is similar to that of **8**. The amounts were as follows: 74.2 mg (0.186 mmol) of [Cu(CH_3CN)$_4$](*p*-CH_3−C_6H_4−SO_3) and 50.0 mg (0.186 mmol) of the ligand bpz*pm. Yield 81.6 mg (87%). **12** is red in color. Anal. Calcd for **12·CH_2Cl_2.** 47.39; H, 4.43; N, 15.41; S, 5.88. Found: C, 47.66; H, 4.70; N, 15.62; S, 5.78. ^{1}H NMR ($CDCl_3$, 300 MHz, 25 °C): δ = 9.13 (s, 1H, H^2), 7.88 (s, 1H, H^5), 7.66 (bs, 2H, H$^{2''}$,6$''$), 7.19 (bs, 2H, H$^{3''}$,5$''$), 6.23 (s, 2H, H$^{4'}$), 2.76 (s, 6H, Me$^{5'}$), 2.39 (bs, 3H, Me$''$), 2.17 (s, 6H, Me$^{3'}$) ppm. IR (Nujol) ν/cm^{-1} 1599(ν(C═N)), 1214, 1200, 1166, 1033, 1009, 817, 680, 567 (*p*-CH_3−C_6H_4−SO_3). UV−vis (CH_2Cl_2) λ (ϵ): 260 (8.83 × 10^4), 297 (1.15 × 10^5), 387 (7.69 × 10^3) nm. MS (FAB$^+$, NBA): *m*/*z* (rel. int. %): 1061 [M^+-bpz*pm-3$C_7H_7SO_3$, 0.3], 1165 [M^+-Cu-bpz*pm-3$C_7H_7SO_3$, 0.2], 977 [M^+-Cu-3bpz*pm-$C_7H_7SO_3$, 0.1], 897 [M^+-Cu-2bpz*pm-3$C_7H_7SO_3$, 0.6], 835 [M^+-2Cu-2bpz*pm-3$C_7H_7SO_3$, 1.1], 615 [M^{2+}-bpz*pm-3$C_7H_7SO_3$, 3.0], 599 [M^+-3Cu-2bpz*pm-4$C_7H_7SO_3$, 57.3], 497 [M^{2+}-Cu-bpz*pm-4$C_7H_7SO_3$, 25.9], 331 [M^+-3Cu-3bpz*pm-4$C_7H_7SO_3$, 100.0] D.

[Cu(Mebpzpm)]$_4$(PF_6)$_4$, 13. The synthesis is similar to that of **2**. In this case, the amounts were as follows: 77.5 mg (0.208 mmol) of [Cu(CH_3CN)$_4$](PF_6) and 50.0 mg (0.208 mmol) of the ligand Mebpzpm. The complex was crystallized by diffusion of the starting reagents in a mixture of the following phases: dichloromethane plus [Cu(CH_3CN)$_4$]PF_6)/acetone/diethyl ether plus Mebpzpm. **13** is orange colored. Yield 84.1 mg (90%). Anal. Calcd for **13**: C, 28.68; H, 2.63; N, 15.24. Found: C, 28.11; H, 2.14; N, 14.85. ^{1}H NMR (acetone-d_6, 400 MHz, 25 °C): δ = 8.92 (s, 1H, H^2), 8.80 (s, 2H, H$^{5'}$), 8.55 (s, 1H, H^5), 8.04 (s, 2H, H$^{3'}$), 2.25 (s, 6H, Me$^{4'}$) ppm. IR (Nujol) ν/cm^{-1} 1611(ν(C═N)), 839 (ν(P−F)), 575, 523 (δP−F). MS (FAB$^+$, NBA): *m*/*z* (rel. int. %): 1169 [M^+-2Mebpzpm-PF_6, 0.2], 1119 [M^+-Mebpzpm-3PF_6, 0.2], 961 [M^+-Cu-2Mebpzpm-2PF_6, 0.3], 749 [M^+-2Cu-2Mebpzpm-3PF_6, 1.3], 543 [M^+-3Cu-2Mebpzpm-4PF_6, 79.7], 366 [M^+-2Cu-3Mebpzpm-4PF_6, 3.1], 303 [M^+-3Cu-3Mebpzpm-4PF_6, 100.0] D.

[Cu(Mebpzpm)]$_4$(BF_4)$_4$, 14. The synthesis of **14** is similar to that of **2**. The amounts were as follows: 65.4 mg (0.208 mmol) of [Cu(CH_3CN)$_4$]BF_4 and 50.0 mg (0.208 mmol) of the ligand Mebpzpm. The complex was crystallized by diffusion in a mixture of the following phases: dichloromethane plus [Cu(CH_3CN)$_4$]BF_4/acetone/diethyl ether plus Mebpzpm. **14** is orange in color. Yield 71.5 mg (88%). Anal. Calcd for **14·1/3CH_2Cl_2**: C, 36.30; H, 3.08; N, 20.95. Found: C, 36.86; H, 3.30; N, 20.74. ^{1}H NMR (acetone-d_6, 400 MHz, 25 °C): δ = 8.92 (s, 1H, H^2), 8.80 (s, 2H, H$^{5'}$), 8.55 (s, 1H, H^5), 8.04 (s, 2H, H$^{3'}$), 2.25 (s, 6H, Me$^{4'}$) ppm. IR (Nujol) ν/cm^{-1} 1608 (ν(C═N)), 1091, 1061 (ν(B−F)), 522 (δ(B−F)). MS (FAB$^+$, NBA): *m*/*z* (rel. int. %): 1476 [M^+-BF_4, 1.4], 1300 [M^+-3BF_4, 0.8], 1085 [M^+-Cu-Mebpzpm-2BF_4, 1.1], 950 [M^+-2Cu-2Mebpzpm, 1.4], 904 [M^+-2Mebpzpm-2BF_4, 2.6], 603 [M^+-Cu-3Mebpzpm-2BF_4, 6.4], 543 [M^+-3Cu-2Mebpzpm-4BF_4, 60.4], 451 [M^+-2Cu-3Mebpzpm-3BF_4, 35.7], 385 [M^+-3Cu-3Mebpzpm-3BF_4, 60.1], 303 [M^+-3Cu-3Mebpzpm-4BF_4, 100.0] D.

[Cu(Mebpzpm)]$_4$(ClO_4)$_4$, 15. The synthesis of this complex is similar to that of **2**. The amounts were as follows: 54.3 mg (0.166 mmol) of [Cu(CH_3CN)$_4$]ClO_4 and 40.0 mg (0.166 mmol) of the ligand Mebpzpm. The complex was crystallized by diffusion in a mixture of the following phases: dichloromethane plus [Cu(CH_3-CN)$_4$]ClO_4/acetone/diethyl ether plus Mebpzpm. **15** is orange in color. Yield 58.4 mg (87%). Anal. Calcd for **15·1/4CH_2Cl_2**: C, , 30,20; H, 2.17; N, 20.12. Found: C, 30.48; H, 2.14; N, 20.36. ^{1}H NMR (acetone-d_6, 400 MHz, 25 °C): δ = 8.96 (s, 1H, H^2), 8.80 (s, 2H, H$^{5'}$), 8.54 (s, 1H, H^5), 8.03 (s, 2H, H$^{3'}$), 2.24 (s, 6H, Me$^{4'}$). IR (Nujol) ν/cm^{-1} 1610 (ν(C═N)), 1098 (ν(Cl−O)), 624 (δ(Cl−O)). MS (FAB$^+$, NBA): *m*/*z* (rel. int. %): 1414 [M^+-2ClO_4, 0.2], 1011 [M^+-Cu-Mebpzpm-3ClO_4, 0.5], 1001 [M^+-2Cu-2Mebpzpm, 0.4], 970 [M^+-Mebpzpm-4ClO_4, 0.6], 947 [M^+-2Cu-Mebpzpm-3ClO_4, 0.7], 890 [M^+-3Mebpzpm, 0.8], 869 [M^+-Cu-2Mebpzpm-2ClO_4, 1.9], 707 [M^+-2Cu-2Mebpzpm-3ClO_4, 3.7], 543 [M^+-3Cu-2Mebpzpm-4ClO_4, 50.4], 401 [M^+-3Cu-3Mebpzpm-3ClO_4, 35.2], 303 [M^+-3Cu-3Mebpzpm-4ClO_4, 100.0] D.

[Cu(ppdMe)]$_4$(PF_6)$_4$, 16. Solutions of ppdMe (58.2 mg, 0.22 mmol) in CH_2Cl_2 (15 mL) and [Cu(CH_3CN)$_4$]PF_6 (80.5 mg, 0.22 mmol) were mixed. The formation of a brown suspension was observed that was stirred at room temperature for 30 min. A partial evaporation under a vacuum and addition to diethyl ether led to the formation of a brown powder, which was isolated by filtration. It was washed with diethyl ether and dried under a vacuum at room temperature. Yield: 94.45 mg (90%). Anal. Calcd. for **16·2/3C_3H_6O**: C, 35.8; H, 3.52; N, 17.27. Found: C, 35.77; H, 3.52; N, 17.19). ^{1}H NMR (acetone-d_6, 400 MHz, 25 °C): δ = 8.69 (s, 2H, H^{4,5}), 6.57 (s, 2H, H$^{4'}$), 2.80 (s, 6H, Me$^{5'}$), 1.83 (s, 6H, Me$^{3'}$) ppm. ^{19}F NMR (acetone-d_6, 300 MHz, 25 °C): δ = −72.8 (d, J = 708 Hz) ppm. ^{13}C{^{1}H} NMR (acetone-d_6, 500 MHz, 25 °C): δ = 152.9 (s, 2C, C$^{3'}$), 151.0 (s, 2C, C^{3,6}), 144.7 (s, 2C, C$^{5'}$), 122.2 (s, 2C, C^{4,5}), 114.4 (s, 2C, C$^{4'}$), 15.3 (s, 2C, Me$^{5'}$), 14.1 (s, 2C, Me$^{3'}$) ppm. IR (Nujol) ν/cm^{-1} 1590 and 1555 (ν(C═N)), 841 (ν(P−F)), 558 (δ(P−F)). UV−vis (CH_2Cl_2) λ (ϵ): 294 (1.09 × 10^5), 362 (2.14 × 10^4), 449 (2.01 × 10^4) nm. MS (FAB$^+$, NBA): *m*/*z* (rel. int. %): 1761 [M^+- PF_6, 2], 1616 [M^+-2PF_6, 2], 807 [M^+-2Cu-2ppdMe-3PF_6, 28], 599 [M^+-3Cu-2ppdMe-4PF_6, 100], 331 [M^+-3Cu-3ppdMe-4PF_6, 88], 269 [M^+-4Cu-3ppdMe-4PF_6, 95] D.

[Cu(ppdMe)]$_4$(BF_4)$_4$, 17. Solutions of ppdMe (60.1 mg, 0.22 mmol) in CH_2Cl_2 (15 mL) and [Cu(CH_3CN)$_4$]BF_4 (70.3 mg, 0.22 mmol) were mixed. The formation of a brown suspension was observed that was stirred at room temperature for 15 min. A partial evaporation in a vacuum and addition to diethyl ether led to the formation of a brown powder, which was isolated by filtration. It was washed with diethyl ether and dried in a vacuum at room temperature. Dark-brown needless were obtained by dissolving the product in acetone and a diffusion of pentane. Yield 86.35 mg (92%). Anal. Calcd for **17·CH_2Cl_2**: C, 38.91; H, 3.78; N, 19.10. Found: C, 38.90; H, 3.87; N, 19.60. ^{1}H NMR (acetone-d_6, 400

MHz, 25 °C): δ = 8.72 (s, 2H, $H^{4,5}$), 6.53 (s, 2H, $H^{4'}$), 2.79 (s, 6H, $Me^{5'}$), 1.85 (s, 6H, $Me^{3'}$) ppm. ^{19}F NMR (acetone-d_6, 300 MHz, 25 °C): δ = −152.0 ppm. $^{13}C\{^1H\}$ NMR (acetone-d_6, 500 MHz, 25 °C): δ = 152.7 (s, 2C, $C^{3'}$), 151.0 (s, 2C, $C^{3,6}$), 144.8 (s, 2C, $C^{5'}$), 122.5 (s, 2C, $C^{4,5}$), 114.2 (s, 2C, $C^{4'}$), 15.2 (s, 2C, $Me^{5'}$), 14.1 (s, 2C, $Me^{3'}$) ppm. IR (Nujol) ν/cm^{-1} 1597 (ν(C═N)), 1068, 1039 (ν(B−F)), 522 (δ(B−F)). UV−vis (CH_2Cl_2) λ (ϵ): 291 (1.07 × 10^5), 357 (2.14 × 10^4), 443 (1.98 × 10^4) nm. MS (FAB^+, NBA): *m*/*z* (rel. int. %): 1587 [M^+-BF_4, 1], 1500 [M^+-$2BF_4$, 2], 599 [M^+-3Cu -2ppdMe-$4BF_4$, 77], 331 [M^+-3Cu-3ppdMe-$4BF_4$, 37], 269 [M^+-4Cu-3ppdMe-$4BF_4$, 100] D.

[Cu(ppdMe)]$_4$(*p*-CH_3−C_6H_4−SO_3)$_4$, 18. Solutions of ppdMe (34.7 mg, 0.13 mmol) in CH_2Cl_2 (15 mL) and [Cu(CH_3CN)$_4$](*p*-CH_3−C_6H_4−SO_3) (51.4 mg, 0.13 mmol) were mixed. The formation of a brown suspension was observed that was stirred at room temperature for 1 h. A partial evaporation in a vacuum and addition to diethyl ether led to the formation of a brown powder, which was isolated by filtration. It was washed with diethyl ether and dried in a vacuum at room temperature. The solid was recrystallized using a mixture of dichloromethane and acetone to solve it and pentane to precipitate. Yield: 56.49 mg (87%). Anal. Calcd for **18·2CH$_2$Cl$_2$**. C, 47.34; H, 4.43; N, 15.41. Found: C, 47.29; H, 4.88; N, 15.23. ^1H NMR (acetone-d_6, 400 MHz, 25 °C): δ = 9.14 (s, 2H, $H^{4,5}$), 6.45 (s, 2H, $H^{4'}$), 2.84 (s, 6H, $Me^{5'}$), 1.88 (s, 6H, $Me^{3'}$) ppm. ^1H NMR ($CDCl_3$, 400 MHz, 25 °C): δ = 9.13 (s, 2H, $H^{4,5}$), 7.81 (bs, 2H, $H^{2''}$, 6″), 7.13 (bs, 2H, $H^{3''}$, 5″), 6.14 (s, 2H, $H^{4'}$), 2.83 (s, 6H, $Me^{5'}$), 2.34 (bs, 3H, Me″), 1.80 (s, 6H, $Me^{3'}$) ppm. $^{13}C\{^1H\}$ NMR ($CDCl_3$, 500 MHz, 25 °C): δ = 151.4 (s, 2C, $C^{3'}$), 150.0 (s, 2C, $C^{3,6}$), 144.2 (s, 2C, $C^{5'}$), 139.5 (s, 1C, $C^{4''}$), 128.8 (s, 2C, $C^{2''}$,6″), 126.2 (s, 2C, $C^{3'',5''}$), 123.0 (s, 2C, $C^{4,5}$), 112.9 (s, 2C, $C^{4'}$), 21.4 (s, 1C, Me″), 15.5 (s, 2C, $Me^{5'}$), 14.2 (s, 2C, $Me^{3'}$) ppm. IR (Nujol) ν/cm^{-1} 1585 (ν(C═N)); 1216, 1163, 1032, 1010, 816, and 566 (CH_3−C_6H_4−SO_3). UV−vis (CH_2Cl_2) λ (ϵ): 289 (1.00 × 10^5), 354 (1.97 × 10^4), 441 (1.73 × 10^4) nm. MS (FAB^+, NBA): *m*/*z* (rel. int. %): 1069 [M^+-Cu-2ppdMe-$2C_7H_7SO_3$, 0.1], 801 [M^+-Cu-3ppdMe-$2C_7H_7SO_3$, 1], 599 [M^+-3Cu-2ppdMe-$4C_7H_7SO_3$, 34], 565 [M^+-2Cu-3ppdMe-$3C_7H_7SO_3$, 10], 331 [M^+-3Cu-3ppdMe-$4C_7H_7SO_3$, 100], 269 [M^+-4Cu-3ppdMe-$4C_7H_7SO_3$, 6] D.

X-ray Structure Determination. Orange crystals of **2** were obtained by diffusion of the starting reagents in a mixture of the following phases: [Cu(CH_3CN)$_4$]PF_6 in dichloromethane/acetone/bpzpm in dibuthyl ether. Red crystals of **3** were obtained by diffusion of the starting reagents in a mixture of the following phases: [Cu(CH_3CN)$_4$]BF_4 in dichloromethane/acetone/bpzpm in diethyl ether. Red crystals of **9** were obtained by recrystallization from 1,2-dichloroethane/hexane. Dark-brown needles of **16** and dark-brown rhombic needles of **18**, respectively, were obtained by recrystallization from acetone/pentane.

X-ray data of **2**, **3**, **9**, **16**, **18** were collected with Bruker Smart CCD area detector diffractometers at T = 173 K using graphite-monochromated Mo−Kα radiation (λ = 0.71073 Å, sealed X-ray tube) and 0.3° ω-scan frames covering either hemispheres or complete spheres of the reciprocal space up to θ_{max} = 25−27°. Corrections for absorption, $\lambda/2$ effects, and crystal decay were applied.[40] After structure solution with program *SHELXS97* refinement on F^2 was carried out with the program *SHELXL97*.[41] Non-hydrogen atoms were refined anisotropically. All of the hydrogen atoms were placed in calculated positions and thereafter treated as riding. A significant issue with all of the structures was their considerable content of mixtures of solvents and the notorious disorder of the solvent molecules. After elaborate attempts to include discrete solvent molecular entities in the refinement, it was found advantageous to *squeeze* the solvents with program *PLATON*,[42] except for **2**, where acetone and dichloromethane could be reasonably fixed. Salient crystallographic data are summarized in Table 1, and further details can be found in the supporting informations in CIF format. Selected geometric data are presented in Table 2.

(40) Bruker programs: *SMART*, version 5.625; *SAINT*, version 6.54; *SADABS*, version 2.10; *SHELXTL*, version 6.1 (Bruker AXS Inc.: Madison, WI, 2003).

(41) Sheldrick, G. M. *SHELX97: Program System for Crystal Structure Determination*; University of Göttingen: Göttingen, Germany, 1997.

Results and Discussion

The ligands bpzpm, bpz*pm, Mebpzpm, and ppdMe (Chart 2) were synthesized from sodium pyrazolate or dimethylpyrazolate and the corresponding dichloro-pyrimidine or -pyridazine heterocycles. The reaction of [Cu(CH_3CN)$_4$]X[39] (X = PF_6, BF_4, ClO_4) with the different ligands in a 1:1 ratio leads to the formation of the new **2**−**4**, **8**−**10**, **13**−**17** complexes (Scheme 1). With the aim of obtaining derivatives with other types of anions like triflate and *p*-toluensulfonate, we tried to synthesize the starting acetonitrile Cu(I) derivatives with these counteranions. These complexes have not been previously described. However, the products obtained were neither easy to crystallize nor were they obtained in pure form. Because of that, we looked for another method and performed the reaction between the ligands and CuCl with the idea of substituting the chloride by the targeted anions, with the aid of the corresponding silver salts. In the case of the ligands bpzpm and bpz*pm, the chloride complexes [Cu(N−N′)Cl]$_n$ (**1**,**7**) were obtained, and the substitution of the anions was possible (Scheme 1). To evaluate which method leads to better yields, **10** was obtained by the two different ways. Starting from CuCl and considering that, in both methods two reaction steps are necessary, the total yield was calculated. For the method that implies the formation of the [Cu(CH_3CN)$_4$]ClO_4 salt (from CuCl and $HClO_4$), the total yield was 68%, and when the chloride intermediate product is previously formed, the total yield was 41%. Consequently, when the acetonitrile adduct is obtained without difficulty, this is the preferred method. In the case of the ppdMe ligand, the chloride derivative is not formed in pure form, and in this case, we reacted the [Cu(CH_3CN)$_4$]-*p*-CH_3(C_6H_4)SO_3 adduct with the ligand, and product **18** was subsequently recrystallized.

The complexes are insoluble in hexane or THF, and their solubility in polar solvents such as acetone or dichloromethane follows the order ppdMe ≫ bpz*pm > bpzpm > Mebpzpm. In more-coordinating solvents such as DMSO, acetonitrile, or even methanol, the tetranuclear structure is broken and free ligand is detected in solution. Derivatives **1** and **7** are more insoluble, and they also have different colors than the other derivatives. In general, the complexes are stable in solution under an inert atmosphere using the Schlenk techniques. However, the derivatives containing chloride or *p*-toluensulphonate are more prone to oxidation, and after about 3−4 h in solution, the color slowly changes to blue-green and broad signals appear in the ^1H NMR spectrum.

(42) Spek, A. L. *PLATON: A Multipurpose Crystallographic Tool*; University of Utrecht: Utrecht, The Netherlands, 2003.

Table 1. Crystal Data and Structure Refinement for **2**, **3**, **9**, **16**, and **18**

	2	**3**[b]	**9**[b]	**16**[b]	**18**[b]
empirical formula	$C_{40}H_{32}Cu_4F_{24}N_{24}P_4 \cdot -2C_3H_6O \cdot 2CH_2Cl_2$	$C_{40}H_{32}B_4Cu_4F_{16}N_{24}$	$C_{56}H_{64}B_4Cu_4F_{16}N_{24}$	$C_{56}H_{64}Cu_4F_{24}N_{24}P_4$	$C_{84}H_{92}Cu_4N_{24}O_{12}S_4$
fw	1968.94	1450.30	1674.71	1907.35	2012.22
T (K)	173(2)	173(2)	173(2)	173(2)	173(2) K
cryst size (mm^3)	0.50 × 0.40 × 0.10	0.34 × 0.16 × 0.14	0.40 × 0.37 × 0.35	0.48 × 0.15 × 0.11	0.71 × 0.30 × 0.22
cryst system	tetragonal	monoclinic	orthorhombic	orthorhombic	monoclinic
space group	$P4_32_12$	$C2/m$	$Ccca$	$Pna2_1$	$P2_1/n$
Z	4	4	4	4	4
a (Å)	16.524(3)	23.745(4)	17.3669(13)	15.8728(16)	13.4233(6)
b (Å)	16.524(3)	15.835(3)	25.742(2)	48.079(5)	33.8902(15)
c (Å)	29.684(5)	18.561(3)	19.5594(15)	12.0564(12)	22.0612(9)
β (deg)	90	111.977(3)	90	90	99.731
V ($Å^3$)	8105(3)	6472(2)	8744(1)	9201(2)	9891.6(7)
ρ_{calcd} (g/cm^3)	1.614	1.488	1.272	1.377	1.351
μ_{calc} (mm^{-1})	1.353	1.392	1.040	1.076	1.000
F(000)	3920	2880	3392	3840	4160
Θ max (deg)	25.0	26.4	26.4	25.7	27.0
total reflns measured	32 261	18 933	24 450	49 932	119 571
indep. reflns: all [R(int)]	7097 [0.089]	6839 [0.061]	4471 [0.0405]	15 409 [0.145]	21 477 [0.035]
[$I > 2\sigma(I)$]	5083	3426	2751	7785	16 615
params refined, restraints	521, 172	430, 160	241, 74	1025, 456	1171, 396
Final $R1$ [$I > 2\sigma(I)$]/ all data[a]	0.0838 / 0.1214	0.0602/0.1172	0.0474/0.0768	0.0675 / 0.1435	0.0557/0.0716
Final $wR2$ [$I > 2\sigma(I)$]/ all data[a]	0.2002/0.2287	0.1587/0.1768	0.1402/0.1531	0.1402/0.1599	0.1543/0.1670
GOF on F^2	1.093	0.919	0.998	0.947	1.081
largest diff. peak and hole e.$Å^{-3}$	1.14 and −0.49	0.75 and −0.57	0.53 and −0.43	0.81 and −0.52	1.29 and −1.25

[a] $R1 = \sum||F_0| - |F_c||/\sum|F_0|$ and $wR2 = \{\sum[w(F_0^2 - F_c^2)]/\sum[w(F_0^2)^2]\}^{1/2}$ [b] Disordered solvent was *SQUEEZED* with program *PLATON*.[42] Chemical formula and derived quantities fw, ρ_{calcd}, μ_{calc}, and F(000) are given without solvent contribution.

Table 2. Selected Bond Distances (Angstroms) and Bond Angles (Degrees) for the $[Cu_4L_4]^{4+}$ Cations of **2**, **3**, **9**, **16**, and **18**

2		**3**		**9**		**16**[a]		**18**[a]	
				Distances					
Cu1−N1	1.974(8)	Cu1−N1	1.975(4)	Cu1−N1	1.966(3)	Cu1−N1	1.999(7)	Cu1−N44	1.971(2)
Cu1−N3	2.084(7)	Cu1−N9	2.011(3)	Cu1−N3	2.063(2)	Cu1−N3	2.023(7)	Cu1−N11	1.980(2)
Cu2−N6	1.970(7)	Cu1−N7	2.033(4)	Cu2−N6	1.971(3)	Cu1−N13	2.006(8)	Cu1−N46	1.996(2)
Cu2−N7	1.989(7)	Cu1−N3	2.061(4)	Cu2−N4	2.059(2)	Cu1−N15	1.981(7)	Cu1−N13	1.999(2)
Cu2−N9	2.067(7)	Cu2−N6	1.990(4)			Cu2−N19	1.985(7)	Cu2−N21	2.001(2)
Cu2−N4	2.071(8)	Cu2−N12	2.031(4)			Cu2−N4	1.995(7)	Cu2−N14	2.008(2)
Cu3−N12	1.985(7)	Cu2−N10	2.033(5)			Cu2−N21	1.995(7)	Cu2−N16	2.018(2)
Cu3−N10	2.094(7)	Cu2−N4	2.053(4)			Cu2−N6	2.019(7)	Cu2−N23	2.020(2)
				Angles					
N1−Cu1−N3	80.7(3)	N9−Cu1−N7	80.24(15)	N1−Cu1−N3	78.97(9)	N15−Cu1−N13	78.7(3)	N44−Cu1−N46	80.30(10)
N7−Cu2−N9	81.1(3)	N1−Cu1−N3	80.80(16)	N6−Cu2−N4	78.88(9)	N1−Cu1−N3	79.0(3)	N11−Cu1−N13	79.61(9)
N6−Cu2−N4	80.1(3)	N6−Cu2−N4	80.21(16)			N19−Cu2−N21	80.0(3)	N14−Cu2−N16	78.76(9)
N12−Cu3−N10	80.2(3)	N12−Cu2−N10	80.09(18)			N4−Cu2−N6	79.1(3)	N21−Cu2−N23	79.74(9)

[a] Only half of the Cu−N distances and bite angles are given. For complete data see the Supporting Information.

The elemental analyses of the new complexes are reflected in the experimental section. In all of the cases, the stoichiometry was Cu/L/X = 1:1:1 (X = anion). The solvents included in the analyses have been detected in the corresponding NMR spectra. The FAB^+ mass spectra are very illustrative of the nuclearity of the new derivatives. In the vast majority of cases, peaks corresponding to fragments with four copper centers such as $[Cu_4L_4X_3]^+$ or $[Cu_4L_4X_2]^+$ were observed. Usually fragments with three copper atoms were also present, and peaks corresponding to the consecutive loss of anions could be detected. The base peaks usually correspond to the fragment $[CuL]^+$ and in some cases to $[CuL_2]^+$. It is noteworthy that for **1**, where the anion is chloride, a peak with high intensity corresponds to the fragment $[CuLCl]^+$ and the base peak corresponds to L^+.

Considering the elemental analyses and the data from the mass spectra for the new complexes, the formation of tetranuclear species with [2 × 2] grid-shaped structures as depicted in Chart 3 is proposed. This has been confirmed by different X-ray structures (below).

The IR spectra show in all cases intense bands in the region of 1600 cm^{-1}, corresponding to the ν(C═N) stretching vibrations of the heterocycles and also to the expected bands for the different counteranions.[43] In the case of the BF_4^- complexes, the band around 1050−1070 cm^{-1} is split. This is an indication of a reduction of the tetrahedral symmetry probably due to interactions of some fluorine with other

(43) Nakamoto, K. In *Infrared and Raman Spectra of Inorganic and Coordination Compounds, 4th ed.*; John Wiley and Sons: New York, 1986; Part II, p 130ss.

Scheme 1

$$4\,[Cu(CH_3CN)_4]X + 4\,L \longrightarrow [CuL]_4X_4 + 16\,CH_3CN$$

L = bpzpm, X = PF_6, **2**; BF_4, **3**; ClO_4, **4**.
L = bpz*pm, X = PF_6, **8**; BF_4, **9**; ClO_4, **10**.
L = Mebpzpm, X = PF_6, **13**; BF_4, **14**; ClO_4, **15**.
L = ppdMe, X = PF_6, **16**; BF_4, **17**; *p*-$CH_3(C_6H_4)SO_3$, **18**.

$$n\,CuCl + n\,L \longrightarrow [CuL]_nCl_n \quad L = bpzpm,\ \mathbf{1};\ bpz^*pm,\ \mathbf{7}.$$
$$\downarrow n\,AgX$$
$$n/_4[CuL]_4X_4 + n/_4\,AgCl$$

L = bpzpm, X = OTf, **5**; *p*-$CH_3(C_6H_4)SO_3$, **6**.
L = bpz*pm, X = ClO_4, **10**; OTf, **11**; *p*-$CH_3(C_6H_4)SO_3$, **12**.

atoms of the molecules. For the chloride derivatives, **1** and **7**, weak bands at 239 and 227 cm^{-1}, respectively, that can be assigned to ν(Cu−Cl) vibrations are observed.[44] Taking into account all of the data, we consider that the tetranuclear nature of the chloride derivatives is not completely established, and the presence of oligomeric chains cannot be excluded.

Solid-State Characterization. X-ray Structures of 2, 3, 9, 16, and 18. The molecular structures of **2**, **3**, **9**, **16**, and **18** have been determined by the corresponding X-ray diffraction studies. The crystallographic data are given in Table 1, and a selection of bond distances and angles are compiled in Table 2. Table 3 gathers some specific angles and distances that are important for the structure discussions. The corresponding ORTEP representations of the tetranuclear cations can be found in part a of Figures 1−5, and a different perspective that also includes some counteranions is shown in part b of Figures 1−3. All of these complexes are tetranuclear, constituted by four CuL units with a grid structure [2 × 2]. The cationic charge is neutralized by four counteranions, and different crystallization solvents are trapped in free spaces of the crystal lattices, the solvent accessible volumes[42] of which vary between 15 (**18**) and 36% (**2**) of the unit-cell volumes. The copper atoms have a distorted tetrahedral environment by each two nitrogen atoms of two chelating ligands. The Cu−N bond distances are in the expected range and are all quite similar, with values between 1.96 and 2.09 Å, with the largest values found for the Cu−N(pm) bonds, in accordance with the lower basicity of the pyrimidine ring. The N−Cu−N angles values vary between 79 and 145°, with low and fairly constant values for the chelating angles (mean value for all five complexes 79.7(7)°) and large and varied values for nonchelating angles (mean value 126(8)°). With respect to copper coordination, no significant difference between **2**, **3**, **9**, **16**, and **18** could be seen. The observed diversity of N−Cu−N bond angles suggests a broad tolerance in the coordination sphere of the copper centers, which could lead to structural flexibility, favorable for the encapsulation properties. The trianular ligands in **2**, **3**, **9**, **16**, and **18** show essentially normal bond lengths and angles, the details of which can be found in the Supporting Information. All of the ligands are approximately flat but show in some cases very significant deviations from

Chart 3

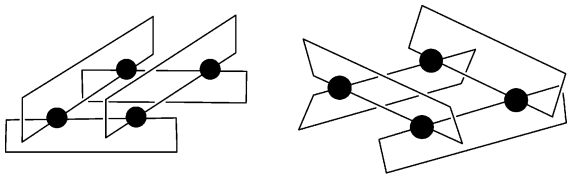

Grids with ppdMe Grids with bpz´pm

planarity by bending and/or twisting, which may be caused by various packing influences. This is particularly true for one ligand in **16** where a pyrazole ring is notably turned out of the common plane of the other two rings because of a short intermolecular contact to a neighboring PF_6^- anion and for two ligands in **18**, which show a distinct curvature that could be related to a trapped solvent. Before entering individual geometric considerations, it should be recalled that the $[Cu_4L_4]^{4+}$ units with [2 × 2] grid structures may ideally adopt the point symmetry $-42m \equiv D_{2d}$, having four symmetry-equivalent copper atoms with a point symmetry of 2 that are arranged in a perfect square, and four symmetry-equivalent ligands L with a point symmetry of *m*. This symmetry is most closely approached by the $[Cu_4L_4]^{4+}$ units in **2** and **3**, but the factual crystallographic point symmetry in **2** is $2 \equiv C_2$, whereas in **3** it is $m \equiv C_s$. The $[Cu_4L_4]^{4+}$ cation in **9** shows, instead of the quadratic, a rhombus-type Cu_4 arrangement, and the complex has here a crystallographic point symmetry of $222 \equiv D_2$. Thus, in all three cases, **2**, **3**, and **9**, the arrangement of the four copper atoms of each complex is, by symmetry requirements, perfectly planar. This is different from the $[Cu_4L_4]^{4+}$ units in **16** and **18**, which both have a point symmetry of 1 and are showing notably nonplanar, flat disphenoidal arrangements of the four copper atoms, as outlined below (see also Table 3).

For **2**, **3**, and **9**, the Cu−Cu distances in the [2 × 2] grid are about 6.1 Å, with Cu−Cu−Cu angles either close to 90° (**2**, **3**) or 79/101° (**9**). As a result of the spatial disposition of the two pairs of chelating nitrogen atoms in each bpzpm/bpz*pm (**2**, **3** and **9**), the ligands are not perpendicular to the Cu_4 quadrangles, rather than inclined to them at angles of ideally near 60°. Thus, the ligand pairs on each side of the complexes adopt divergent orientations, which leads to the formation of two groove-like cavities for each complex, which are occupied by two PF_6 (**2**) or two BF_4 anions (**3**, **9**). In the space filling diagram of **2** that is given in Figure 6, the two encapsulated PF_6^- that are symmetry equivalent are clearly seen. Because of the above-mentioned flexibility of the copper coordination figures, the angles between opposite ligand pairs vary notably and thus help to host, or even to complex, the two anions. Thus, in **9**, a low interplanar angle of 27.8(1)° (Table 3) is observed, whereas the corresponding angle in **3** on one side of the Cu_4 quadrangle is 42.8(1) and on the other side is 78.0(1)°. One possible driving force behind these variations is the interaction of the anions with the walls of the $[Cu_4L_4]^{4+}$ cations. Considering the distances found between fluorine atoms and the centroids of the pyrimidine rings, there are tight contacts between the fluorine atoms of the PF_6/BF_4 anions and the π-electron density of this ring of the ligand (F···π interactions). In **2**,

(44) Troy, D.; Legros, J. P.; McQuillan, G. P. *Inorg. Chim. Acta* **1983**, *72*, 119.

Table 3. Selected Geometric Parameters for the $[Cu_4L_4]^{4+}$ Cations of Complexes of **2**, **3**, **9**, **16**, and **18**

complex	point symmetry of the $[Cu_4L_4]^{4+}$ unit	Cu—Cu distances (Å)	Cu—Cu—Cu angles (deg)	aplanarity[a] of Cu_4 quadrangle (Å); shape	aplanarity[a] of the ligands (Å)	angle between opposite ligands planes (deg)	cavity size (Å) L; W (for **2**, **3**, and **9**)[b] centroid to plane distances (**16** and **18**)[c]
2	$2 \equiv C_2$	6.216 (2×)	99.95	0	0.036 (2×)	41.7(1)	8.38; 6.36
		6.212 (2×)	90.01	~square	0.033 (2×)		
			90.02 (2×)				
3	$m \equiv C_s$	6.027	90.36 (2×)	0	0.046	42.8(1)	9.43; 6.10
		6.103	89.64 (2×)	~square	0.123		8.48; 6.58
		6.145 (2×)			0.092 (2×)	78.0(1)	
9	$222 \equiv D_2$	6.106 (4×)	79.21 (2×)	0	0.107 (4×)	27.8(1)	7.82; 6.25
			100.79 (2×)	rhombus			
16	$1 \equiv C_1$	3.595	81.89	0.274 distorted disphenoid	0.094	3.9(1)	3.41 and 3.45
		3.603	95.19	distorted disphenoid	0.089		
		3.585	82.25		0.192	4.5(1)	3.51 and 3.50
		3.586	95.31		0.115		
18	$1 \equiv C_1$	3.611	83.95	0.212	0.021	1.1(1)	3.43 and 3.42
		3.582	93.90	distorted disphenoid	0.038		
		3.580	84.03		0.260	1.2(1)	3.39 and 3.40
		3.556	94.89		0.222		

[a] Aplanarity is the rms deviation from a common least-squares plane of the corresponding entity; for the ligands, this quantity includes only ring atoms but no methyl groups. [b] See Chart 4 for the definitions of L and W [c] Distance between the centroid of one ligand to the plane of the opposite ligand (central ring).

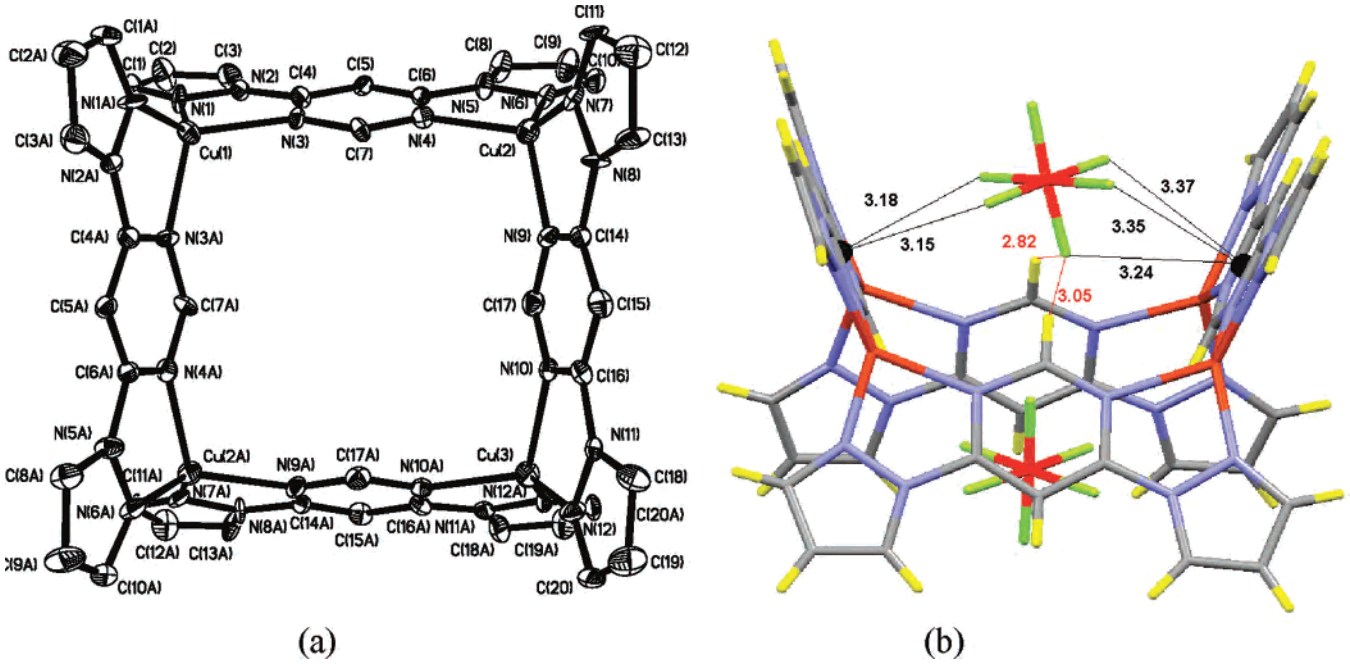

Figure 1. (a) ORTEP representation of the cation of **2**. (b) Stick representation of **2** including the encapsulated anions. Hydrogen bonds are in red. Anion−π interactions are in black.

Chart 4

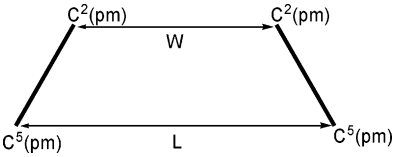

five of the six fluorine atoms of the PF_6 octahedron are remarkably near the pyrimidine rings, with F···π(centroid) distances in the range of 3.15−3.37 Å (from the viewpoint of PF_6 one face- and one edge-sharing contact, part b of Figure 1). A situation comparable is met with BF_4 in **9**. Here, each of the two symmetry-equivalent BF_4 tetrahedra encapsulated by the $[Cu_4L_4]^{4+}$ unit has, via tetrahedral edges, close side-on contacts with two pyrimidine rings (part b of Figure 3), and the rhombus-like distortion of the Cu_4 quadrangle in **9** facilitates these interactions. The respective F···π(centroid) distances found in **3** are 3.15 and 3.18 Å. All of these data are strongly indicative of significant electronic interactions, but must also include Coulomb attraction between anionic and cationic parts. In addition, weak nonclassical hydrogen bondlike C−H···F interactions[45] are also present. In **2**, the bonding is with one specific fluorine of the anion and the C^2H groups of two facing pyrimidine rings, for example, a C(H)···F···(H)C interaction with C···F distances of 3.50

(45) (a) Grepioni, F.; Cojazzi, G.; Draper, S. M.; Scully, N.; Braga, D. *Organometallics* **1998**, *17*, 296. (b) Jeffrey, G. A. In *An Introduction to Hydrogen Bonding*; Oxford University Press: New York, 1997; p 12. (c) Steiner, T. *Angew. Chem., Int. Ed.* **2002**, *41*, 48.

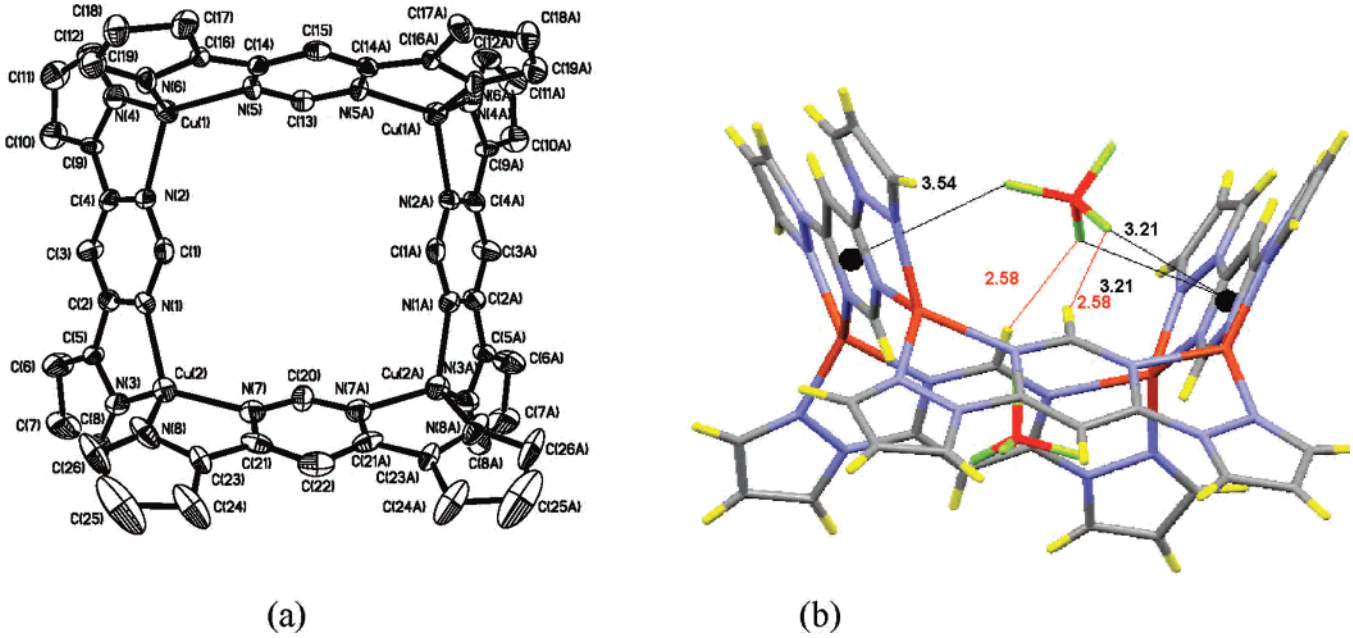

Figure 2. (a) ORTEP representation of the cation of **3**. (b) Stick representation of **3** including the encapsulated anions. Hydrogen bonds are in red. Anion−π interactions are in black.

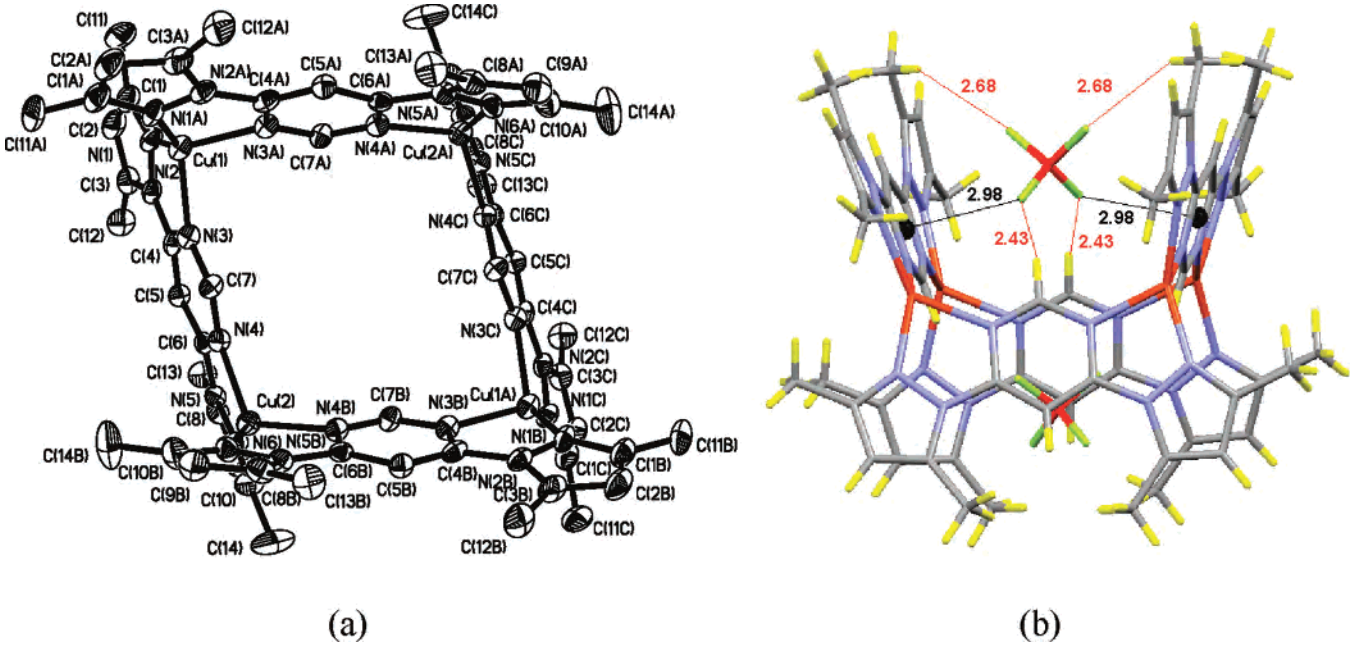

Figure 3. (a) ORTEP representation of the cation of **9**. (b) Stick representation of **9** including the encapsulated anions. Hydrogen bonds are in red. Anion−π interactions are in black.

and 3.70 Å (part b of Figure 1). In **3** and **9**, the interactions that are also with the C^2H pyrimidine groups are of the type C(H)···FBF···(H)C, and the C···F distances vary between 3.07 and 3.70 Å (part b of Figures 2 and 3). Moreover, in **9**, where the ligand has methylated pyrazolyl groups, the other two fluorine atoms of each anion interact with the methyl groups (C···F = 3.38 Å). This may cause the deviation of the involved pyrazoles from the plane of the rest of the ligand.

Compared with **2** and **9**, the cationic $[Cu_4L_4]^{4+}$ group in **3** has an outstanding large angle between opposite ligands of 78° (Table 3). This last feature has been found to be the result of crystal packing, because here adjacent $[Cu_4L_4]^{4+}$ units partly interpenetrate each other in a fashion that gives rise to intermolecular $\pi-\pi$-stacking contacts between the inner sides of pyrazole rings.

For **16** and **18** containing the ppdMe ligand, structural architectures differing markedly from those of the previous complexes have been found. The spatial disposition of the two pairs of chelating nitrogen atoms in the ppdMe ligand causes the $[Cu_4L_4]^{4+}$ moieties to show, first, much-shorter intramolecular Cu−Cu distances, ca. 3.6 Å, (Table 3), and, second, it also favors a nearly parallel alignment of opposite ligands L. As a result of both features, the $[Cu_4L_4]^{4+}$ units

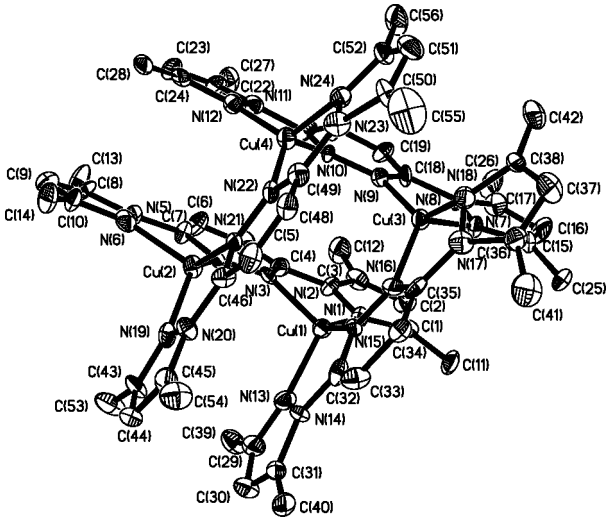

Figure 4. ORTEP representation of the cation of **16**.

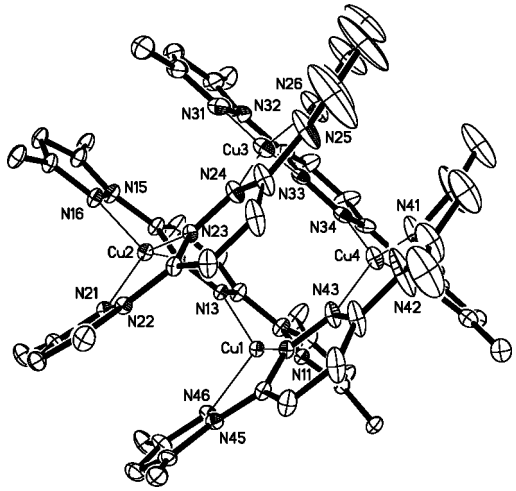

Figure 5. ORTEP representation of the cation of **18**.

of **16** and **18** are very compact, show extended intramolecular $\pi-\pi$-stacking interactions[46] between adjacent ligands, and have no intramolecular cavity to complex counteranions like PF_6 in **16**. The uneven disphenoidal arrangement of the Cu_4 unit, which contrasts the planar Cu_4 units in **2**, **3**, and **9**, is advantageous for the intramolecular $\pi-\pi$-stacking interactions because by this distortion, parallel ligand pairs are not superimposed exactly one above the other but are instead mutually shifted and laterally rotated, which helps to separate the bulky methyl groups and avoids the superposition of equally charged regions of the π-electron surfaces of the ligands. Because of the fact that the ligands in **16** and **18** show mostly quite significant deviations from perfect planarity (ligand aplanarity in Table 3), the data given in the last column of Table 3 provide only a course measure of the $\pi-\pi$-stacking separations (centroid of one ligand to the plane of the opposite ligand distances), which are 3.4−3.5 Å. It must also be mentioned the presence of two $Cu_4L_4-Cu_4L_4$ $\pi-\pi$-stacking interactions in **16** and two pronounced tosylate$-Cu_4L_4$ $\pi-\pi$-stacking interactions in **18**.

(46) (a) Janiak, C. *Dalton Trans.* **2000**, 3885. (b) Mukhopadhyay, U.; Choquesillo-Lazarte, D.; Niclós-Gutierrez, J.; Bernal, I. *Cryst. Eng. Comm.* **2004**, *6*, 627.

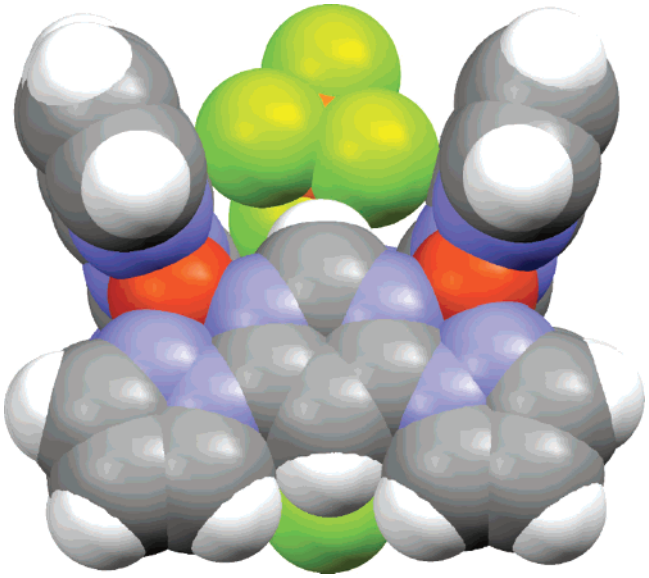

Figure 6. Space filling representation of the $[Cu_4L_4]^{4+}$ moiety in **2** and the two $P(1)F_6$ octahedra entrapped in it (copper orange, nitrogen blue, carbon gray, fluorine green, hydrogen white; in the lower PF_6 octahedron, only one fluorine atom is visible).

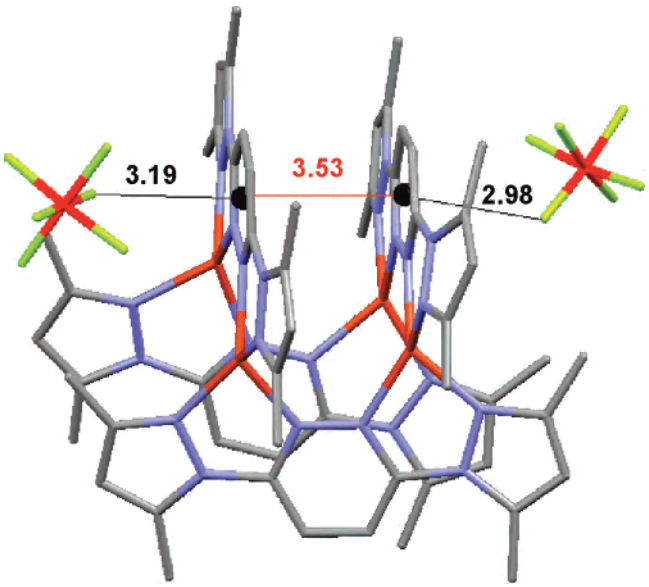

Figure 7. Drawing of the cation of **16** and two anions showing the anion$-\pi$ and $\pi-\pi$ interactions.

For all of the complexes, their $[Cu_4L_4]^{4+}$ entities show a plenitude of C−H···F (**2**, **3**, **9**, and **16**) and C−H···O (**18**) interactions with the surrounding anions, the details of which are outside of the scope of this article. It is noteworthy that there are also anion···π interactions involving the pyridazine rings. These are reflected in Figure 7 for **16** as an example.

In conclusion, it is possible to state that three differences are evident between complexes with pyridazine (**16** and **18**) and those with pyrimidine as the central ring, namely, (i) The four copper atoms of the grids define a square (distorted in some cases to a rhombus) of smaller size for the pyridazine than for the pyrimidine derivatives. (ii) In **16** and **18**, the organic components are distributed in two parallel pairs at a relatively small distance, whereas in the rest, they are divergent and more separated. (iii) In the case of **16** and **18**,

because of the small size of the cavity, there are no counteranions trapped intramolecularly in the $[Cu_4L_4]^{4+}$ unit, and extended intramolecular $\pi-\pi$ stacking interactions are present. However, in **2**, **3**, and **9**, two of the four counteranions are retained in the cavities of these larger and more-open complexes that interact through noncovalent bonds (C−H···F and F···π) with the walls of the tetranuclear entities. As previously proposed, the different placement of the donor atoms in the pyrazine or pyrimidine central rings of the ligands is the main reason for the observed differences. The presence of methyl groups in the pyrazole rings also affects the conformation of the ligands in the grids.

To our knowledge, the structures of **2**, **3**, and **9** represent the first examples of supramolecular grids, where the facing ligands are not parallel, defining cavities of different shape than that of the complexes containing parallel ligands. These cavities are opened toward the outside of the structure and could open new possibilities concerning a host−guest chemistry. Furthermore, these complexes exhibit a high degree of flexibility, a fact that could be favorable in adapting to the substrates.

Solution Behavior. NMR. The ^{1}H, ^{19}F, and ^{13}C{^{1}H} NMR data of the ligands and complexes are reported in the Experimental Section (except for **6**, which was too insoluble) (Table S1 gathers the ^{1}H NMR data along with those of the free ligands to compare the values more easily). The low solubility of some complexes prevented the recording of the corresponding ^{13}C{^{1}H} NMR spectra. When available, the ^{1}H NMR data are indicated in different solvents to do proper comparisons. In all of the complexes and in both ^{1}H and ^{13}C{^{1}H} NMR spectra, signals for only one type of central ring and one type of pyrazole are observed, reflecting the high symmetry of the derivatives. For the corresponding assignments, besides bibliographic information,[47] NOEs, HMQC, and also HMBC experiments have been made in some cases.

For complexes that contain the ligand bpzpm, the differentiation between the protons H$^{3'}$ and H$^{5'}$ of the pyrazole ring has been made,[47] using the fact that $J_{H^5{}'H^{4'}} > J_{H^4{}'H^{3'}}$. In the case of complexes containing the ligand bpz*pm, an NOE between H^5 of the pyrimidine ring and Me$^{5'}$ of the pyrazole heterocycle allows the differentiation between the Me$^{3'}$ and Me$^{5'}$ resonances. Similarly, because of the NOE between Me$^{5'}$ and the H^{4,5} protons of the pyridazine ring, both resonances have been assigned in **16**−**18**. In case of **18**, where the *p*-toluensulfonate anion is present, the corresponding methyl group is identified by its NOE with the H$^{3''}$, H$^{5''}$ protons of the benzene ring (273 K). With the HMQC spectra, the differentiation between the carbons of the Me$^{3'}$ and Me$^{5'}$ groups has been possible, and the quaternary carbons have been assigned by means of the HMBC spectra.

When the chemical shifts of the carbon resonances of the complexes are compared with those of the corresponding free ligands, a general shielding is observed in the pyrimidine (except C^5) or pyridazine carbons and a deshielding of the carbons of the pyrazole rings. In the case of the ^{1}H NMR spectra, usually a shift toward higher frequencies is observed, because of the donation of electron density toward the metal. We note the high change that is observed in the Me^5 resonances of the bpz*pm derivatives. This is due to the fact that, in the free ligand, the pyrazole groups are free to rotate with respect the N(pz*)−C(pm) bond. When the ligand is coordinated, the pyrazolyl rings are forced to be coplanar with the pyrimidine heterocycle, and the Me^5 groups are more affected by the deshielding zone of this last ring.

Complexes containing the counteranions BF_4^-, PF_6^-, ClO_4^-, and OTf^- show very similar ^{1}H NMR chemical shifts (**8** shows a small difference with the others in the H^2(pm) resonance). The low temperature ^{1}H NMR spectra (−80 and −60 °C for acetone-d_6 or $CDCl_3$ solutions, respectively) exhibit the same number of sharp resonances. The fluorine spectra at low temperatures did not show clear changes with respect to those of room temperature, except for **2** and **3** where some slight broadening of the fluorine resonances was observed. A possible explanation of this fact could be the existence of rapid interchange, not completely frozen at low temperature, involving weak cation−anion interactions.

However, a different behavior has been found for the *p*-toluensulfonate and chloride derivatives. The resonances of the complexes with *p*-toluensulfonate have different positions than those of the other derivatives, reflecting in this case an influence of the anion. Besides, the signals of *p*-toluensulfonate are broad at room temperature in all derivatives. For derivative **12**, the signals of the ligand are also broad. At low temperature a small broadening of all of the signals was observed both in acetone-d_6 (−80) as in $CDCl_3$ (−60 °C) for **18**. However, for the pyrimidine derivative, splitting of the signals is observed at low temperature. These facts may indicate the existence of interchange processes in solution.

For the chloride complexes, at room temperature there is observed a clear resonance broadening, especially marked for **7**. At −60 °C, all of the signals expected for a symmetric ligand are observed, and although they are broad, they are clearly sharper than at room temperature. The chemical shifts for the different spectra are very similar to those of the free ligand at the same temperature. This behavior could be due to a competition between the ligand and the chloride toward the coordination to the Cu(I) centers, with a ratio of species changing with temperature. Considering the chemical shifts, it must be accepted that the free ligand is the dominant species. The sharpening of the signals when the temperature decreases points to a higher predominance of one species, in that case, the free ligand. At −60 °C, 4 equiv of free ligand were added to a solution of **7** in acetone-d_6 in an NMR tube. After that, new resonances did not appear, but those existing prior to the addition became sharper and they were shifted toward the chemical shifts of the free ligand. These data support the existence in solution of the stated interchange

(47) (a) Oro, L. A.; Esteban, M.; Claramunt, R. M.; Elguero, J.; Foces-Foces, C.; Cano, F. H. *J. Organomet. Chem.* **1984**, *276*, 79. (b) Esteruelas, M. A.; Oro, L. A.; Apreda, M. C.; Foces-Foces, C.; Cano, F. H.; Claramunt, R. M.; López, C.; Elguero, Begtrup, J. M. *J. Organomet. Chem.* **1988**, *344*, 93. (c) Fajardo, M.; de la Hoz, A.; Díez-Barra, E.; Jalón, F. A.; Otero, A.; Rodríguez, A.; Tejeda, J.; Belletti, D.; Lanfranchi, M.; Pellinghelli, M. A. *J. Chem. Soc., Dalton Trans.* **1993**, 1935.

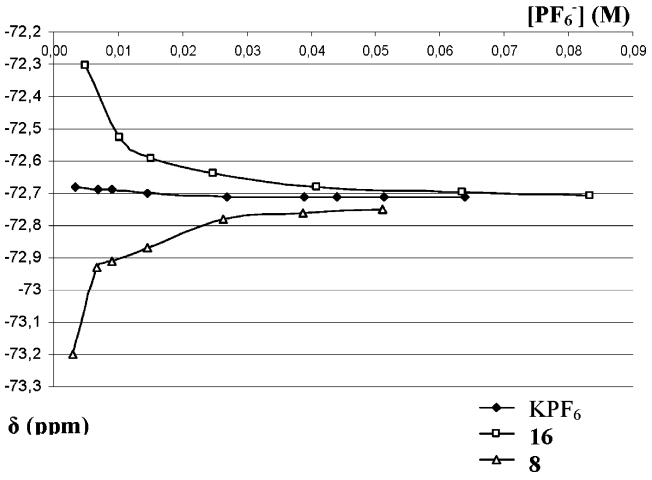

Figure 8. ^{19}F NMR chemical shift for the PF_6^- group in KPF_6, **8** and **16** against the PF_6^- concentration.

between the chloride complexes and the free ligand. This will be confirmed with the UV−vis studies (below).

Other experiments were made to evaluate if there existed interchange between complexes **9** or **16** and their respective ligands in solution. To an acetone-d_6 solution of each complex, there was added successively 1, 2, 3, and 4 equiv of the free ligand. In the case of **9**, when the ligand was added, the spectrum showed broad resonances. This could be due to either a process of interchange between the free ligand and the complex or to a rupture of the tetranuclear structure, giving mononuclear or oligomeric species. To clarify this point, the spectrum of the sample with four ligands per complex was recorded at −80 °C. The resonances were split, and in the region of the $H^{4'}$(pz), at least six signals were observed. In the region of the H^2 and H^5 of the pyrimidine ring, at least four resonances were detected. This indicates that new species have been formed, some of them containing ligands with different pyrazole rings.

The behavior of **16** was different. When the ligand was added in a complex to a ligand ratio from 1:1 to 1:4, the resonances of the complex did not change and the signals of the ligand appeared separately. The respective integration of the resonances corresponded to the amount of complex and ligand added. This indicates that this complex is much more stable than **9**. One reason could be the $\pi-\pi$ stacking found for **16** that could stabilize the grid.

Study of the Cation−Anion Interactions. Diffusion NMR Experiments. A comparative study was made of the variation of the ^{19}F chemical shift of the PF_6^- resonance for a solution of KPF_6 and solutions of **8** or **16** when increasing amounts of KPF_6 were added (Figure 8). For the complexes, the chemical shift of the anion is different to that of KPF_6. This points to the existence of some cation−anion interaction in solution. This is supported by the effect of the KPF_6 addition to the complexes' solutions: the chemical shift changes and it approaches that of the free anion. It is concluded that the chemical shift exhibited by the anion in the complexes is an average of free and interacting anions, reflecting a fast exchange process. The ^1H NMR chemical shifts of the cation did not change in these

Table 4. Values of the Diffusion Coefficients at 298K for the Grid Complexes, Their Counterions, and Internal TMS (as Reference)[a]

	8	**9**	**11**	**16**	**17**
[complex] (mM)	0.74	0.73	0.75	1.22	0.74
$D_{grid}(^1H)$	1.31	1.29	0.99	1.59	0.97
$D_{anion}(^{19}F)$	2.30	2.51	1.96	2.44	1.86
D_{TMS} (^1H)[48]	*4.20*	*4.18*	*3.94*	*4.40*	*3.79*
D_{grid}/D_{TMS}	0.31	0.31	0.25	0.36	0.26
D_{anion}/D_{TMS}	0.55	0.60	0.50	0.55	0.49
$D_{anion\ salt}$ (^{19}F)	2.98	3.13	2.92	2.96	3.13
ρ	0.40	0.34	0.50	0.38	0.59

[a] The diffusion coefficients of the free anion in solution (as the free salt) were recorded at the same counterion concentration as for the grid solutions. D values are listed as 10^{-9} m^2 s^{-1}.

experiments, indicating that the cation−anion interaction is probably weak.

Similar experiments were performed with Bu_4NBF_4 and **9** or **17** with identical results. However, when the study was made with the triflate complex **11** and Bu_4NOTf, the chemical shift of the anion in the complex was similar to that of the ammonium salt and did not suffer changes with its concentration. This can be due to the fact that the counteranion will interact with the grid through the SO_3 group, and the CF_3 fragment is not sensitive enough to these interactions.

We also performed heteronuclear 2D-NOE spectroscopy, more specifically, ^{19}F,^1H-HOESY. In this experiment, correlations between two nuclei are observed if they are close in space. Consequently, it is a useful experiment to determine the interaction between the anion and the tetracationic entities and also to know in which direction it is approaching the counteranion. The experiment was performed for **16**, whereas **8** was not sufficiently soluble. A correlation exists between the fluorine resonance and the signal corresponding to the H^4,H^5 protons of the pyridazine ring. This indicates that the counteranion approaches the tetranuclear fragment from the region of H^4 and H^5 protons of this ring. This is in accordance with the results found in the solid state for the corresponding structure determined by X-ray diffraction (Figure 7).

Diffusion NMR experiments were also performed for **8**, **9**, **11**, **16**, and **17** as an additional approach to investigating complex formation. Diffusion coefficients were determined for the tetracationic entities (^1H measurements) and for their counteranions (^{19}F measurements) in dilute acetone-d_6 solutions (∼1 mM grid). The coefficients for the anions alone as free salts were determined from solutions of KPF_6, NBu_4BF_4, and NBu_4OTf at similar concentrations. The values (Table 4) were smaller for the anions in the complexes (they diffused more slowly) than for the classical salts at similar concentrations but higher than the values of the grids. These data suggest that the anions are not retained by the grids in solution for either the open or closed complexes but do exhibit weak association. The effect of adding increasing amounts of classical salts to the complex solutions was also analyzed and the data for **8** and **16** are shown in Figure 9. The results for both complexes are strikingly similar; the diffusion coefficients of the counteranion initially increased approaching the value of the free anion and then showed a small but progressive decrease at higher salt concentrations

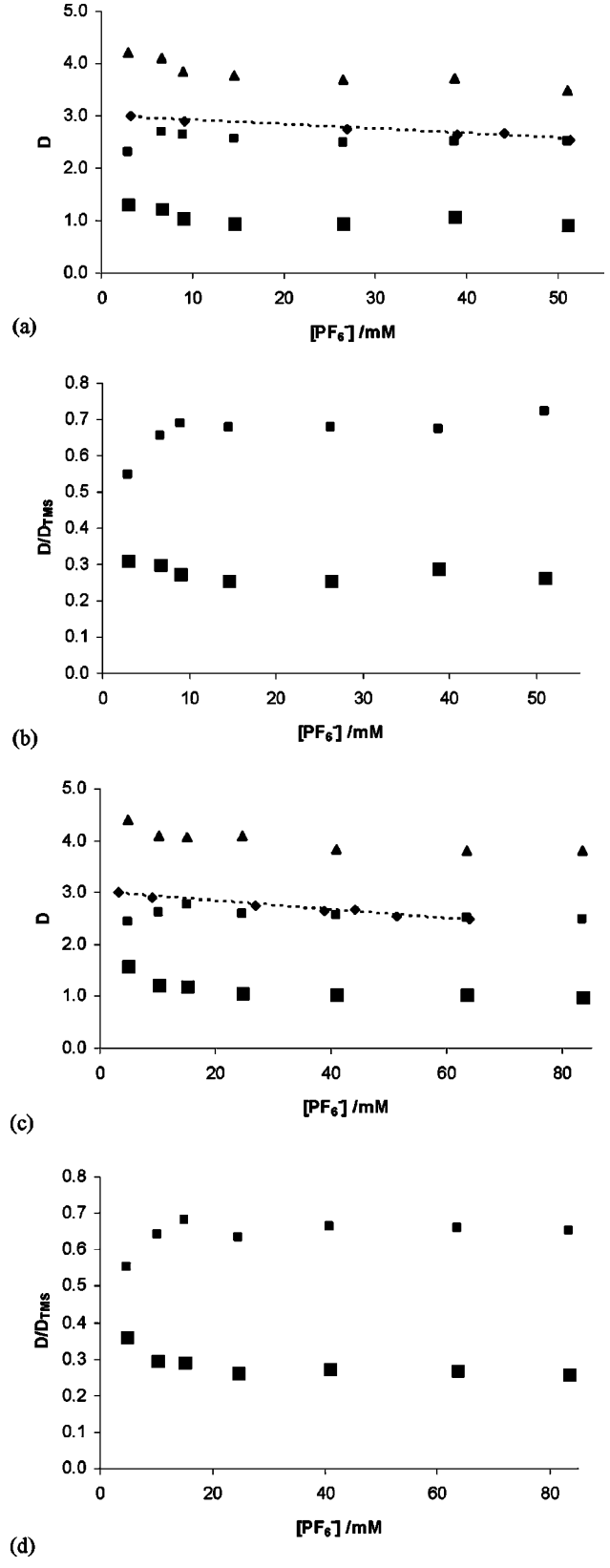

Figure 9. Diffusion titration data for **8** and **16**. (a) and (c): Diffusion coefficients (10^{-9} m^2 s^{-1}) for **8** and **16**, respectively, plotted as a function of total PF_6^- anion concentration for grid and counterion of the complex, for internal TMS and external free anion as KPF_6 (highlighted with a dashed line). (b) and (d): Diffusion coefficients for **8** and **16**, respectively, normalized to those of internal TMS for the grid and counterion. Legend: large square, grid; small square, anion; triangle, TMS; diamond, free anion.

(parts a and c of Figure 9). This behavior is paralleled by the free salt in solution and by the internal reference material (TMS)[48] in the complex solution and suggests higher solution viscosity as the ionic strength increases. The counteranion behavior is more pronounced when its diffusion coefficients are normalized to that of the internal reference (parts b and d of Figure 9).

In contrast, the diffusion values for the grids exhibit a behavior that broadly parallels that of the internal reference, with only a modest decrease observed with increasing anion concentration when normalized to TMS. These small changes may be attributed to a shift in the equilibrium of the interacting anion toward the complexed form at higher concentrations, resulting in a slight retardation of the grid complexes. Similar results were observed for all of the complexes studied (data not shown), and overall these diffusion data indicate that weak cation−anion interactions exist in solution with the counteranions undergoing fast exchange on the diffusion time scale between the free and ion-paired states, behavior consistent with the chemical-shift titration data presented above. Assuming that the observed diffusion coefficients for the grids are similar to those expected for the complexed anions, we have estimated the fraction of bound anions (ρ, Table 4) using the following equation:[49]

$$D_{obs} = \rho D_{complex} + (1 - \rho) D_{free}$$

where D_{free} is the diffusion coefficient for the anion in a classical salt, $D_{complex}$ is the value obtained for the grid, and D_{obs} is the observed value for the anions that should be the weighted average of D_{free} and $D_{complex}$. Values between 0.3 and 0.6 have been obtained, and the similarities for the grids with both types of ligands suggest that those with ppdMe interact with the counteranions even though their cavities are too small to host them, suggesting that ion-pair formation is the dominant interaction for all types of these grid complexes.

UV−Vis. UV−vis spectra were recorded for dichloromethane solutions of the ligands bpz*pm and ppdMe and the corresponding complexes (**7**−**12** and **16**−**18**) (Experimental Section). The complexes with the other ligands were not soluble enough. For the bpz*pm complexes (Figure 10, the concentration is not exactly the same in order to better see the lines, see the values of ϵ in the Experimental Section) it is very illustrative to compare the spectra with that of the free ligand. For the ligand, two bands appear (266 and 293 nm) and a shoulder. For **8**−**11**, the band at 266 nearly disappears and that of 293 nm is slightly red-shifted. In addition, a new and broad band appears at 407 nm with similar values of ϵ for all of the derivatives. This band in the visible region is ascribed to a metal-to-ligand charge transfer (MLCT) transition and is characteristic of copper(I) surrounded in a tetrahedral fashion with four nitrogen atoms.[13b,18a] All of these data are in accordance with the

(48) Cabrita, E. J.; Berger, S. *Magn. Reson. Chem.* **2001**, *39*, S142.
(49) Bakkour, Y.; Vermeersch, G.; Morcellet, M.; Boschin, F.; Martel, B.; Azaroual, N. *J. Inclusion Phenom. Macrocyclic Chem.* **2006**, *54*, 109.

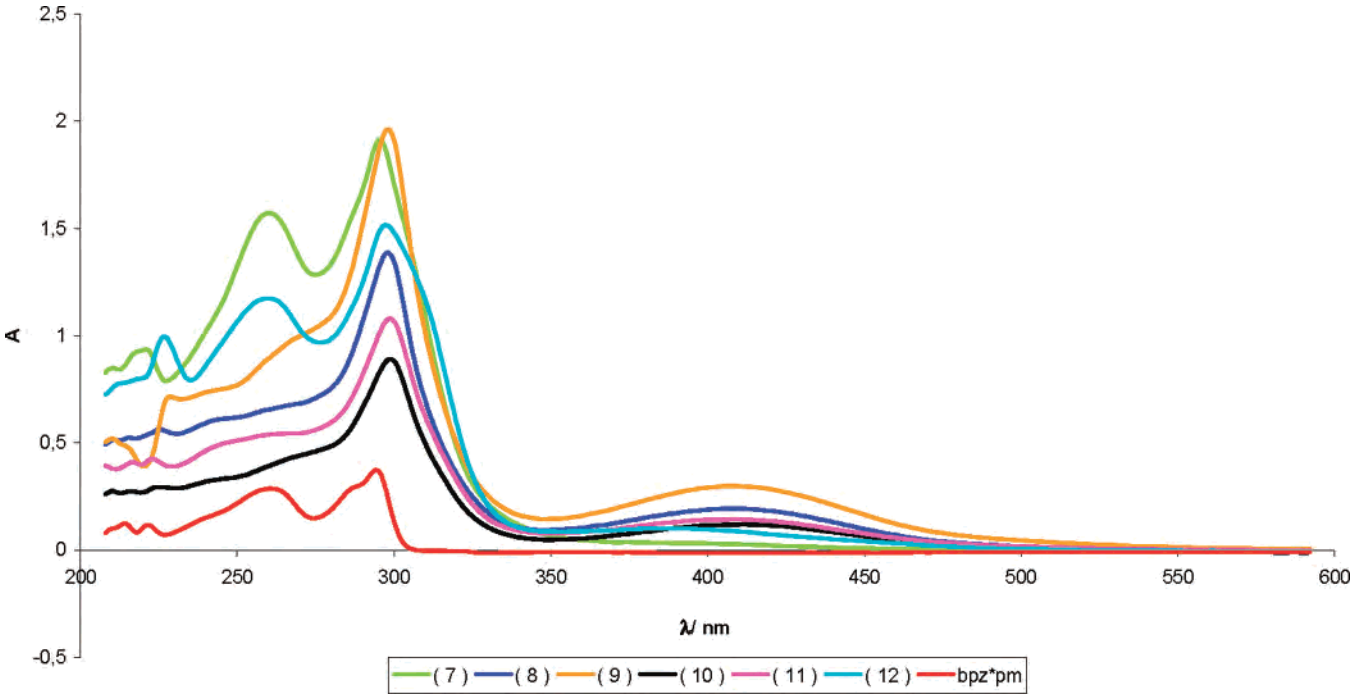

Figure 10. UV−vis spectra of the ligand and complexes indicated (Experimental Section for data).

formation of the new complexes that do not dissociate ligands in a significant amount.

A different situation is found for complexes with chloride (**7**) and *p*-toluensulfonate (**12**), where a band at 260 nm is clearly visible. The other ligand-centered band is less shifted (mainly for **7**) and the MLCT is much less intense (for the chloride complex it has practically disappeared). All of this points to that, for **7** and **12**, an interchange between the complexes and free ligand exists in solution, more shifted to the free ligand for **7**, in accordance with the NMR data.

For the ppdMe complexes (**16**−**18**), the sole band of the free ligand is red-shifted and a MLCT band is clearly visible for the three complexes at 441−449 nm. In this case, the *p*-toluensulfonate complex (**18**) does not show any sign of ligand decoordination.

Conclusions

We have introduced newly designed nitrogenated ligands (bpzpm, bpz*pm and Mebpzpm) for binding to Td centers, to obtain a new type of [2 × 2] metallic grid with divergent facing ligands. The grids obtained contain two open cavities that are able to host two counteranions in the solid state (X-ray structure determinations) that interact with the cationic grid through hydrogen bonds and anion−π interactions involving the pyrimidine rings. The introduction of methyl groups in the pyrazolyl rings induce marked distortions in the disposition of the ligands demonstrating a certain degree of flexibility in the grids. For the sake of comparison, another type of ligand (ppdMe) predesigned to obtain grids with parallel ligands was synthesized. The corresponding [2 × 2] metallic grids have smaller cavities where the anions are not contained and each pair of parallel ligands exhibits aromatic $\pi-\pi$ interactions. We have demonstrated that anion−π interactions are present with the pyridazine rings. The behavior in solution of the new grids obtained was studied by multinuclear NMR, HOESY and diffusion experiments, and UV−vis spectroscopy. Weak cation−counteranion interactions were detected in solution. We are currently investigating the hosting of other type of guests. The results presented here provide a rational approach for the engineering of molecular scaffolding.

Acknowledgment. This work was supported by the DGES of the Ministerio de Educación y Ciencia of Spain (CTQ2005-01430/BQU) and the Junta de Comunidades de Castilla-La Mancha-FEDER Funds (PBI-05-003).

Supporting Information Available: X-ray crystallographic files. Tables S1 and S2 with the ^{1}H and ^{13}C NMR data, respectively, of ligands and complexes. This material is available free of charge via the Internet at http://pubs.acs.org.

IC701117A